RESEARCH ARTICLE

INTERSTELLAR DUST

Evidence for interstellar origin of seven dust particles collected by the Stardust spacecraft

Andrew J. Westphal,[1]* Rhonda M. Stroud,[2] Hans A. Bechtel,[3] Frank E. Brenker,[4] Anna L. Butterworth,[1] George J. Flynn,[5] David R. Frank,[6] Zack Gainsforth,[1] Jon K. Hillier,[7] Frank Postberg,[7] Alexandre S. Simionovici,[8] Veerle J. Sterken,[9,10,11,12] Larry R. Nittler,[13] Carlton Allen,[14] David Anderson,[1] Asna Ansari,[15] Saša Bajt,[16] Ron K. Bastien,[6] Nabil Bassim,[2] John Bridges,[17] Donald E. Brownlee,[18] Mark Burchell,[19] Manfred Burghammer,[20] Hitesh Changela,[21] Peter Cloetens,[22] Andrew M. Davis,[23] Ryan Doll,[24] Christine Floss,[24] Eberhard Grün,[25] Philipp R. Heck,[12] Peter Hoppe,[26] Bruce Hudson,[27] Joachim Huth,[26] Anton Kearsley,[28] Ashley J. King,[23] Barry Lai,[29] Jan Leitner,[26] Laurence Lemelle,[30] Ariel Leonard,[24] Hugues Leroux,[31] Robert Lettieri,[1] William Marchant,[1] Ryan Ogliore,[32] Wei Jia Ong,[24] Mark C. Price,[19] Scott A. Sandford,[33] Juan-Angel Sans Tresseras,[22] Sylvia Schmitz,[4] Tom Schoonjans,[20] Kate Schreiber,[24] Geert Silversmit,[20] Vicente A. Solé,[22] Ralf Srama,[34] Frank Stadermann,[24]† Thomas Stephan,[23] Julien Stodolna,[1] Stephen Sutton,[29] Mario Trieloff,[7] Peter Tsou,[35] Tolek Tyliszczak,[3] Bart Vekemans,[20] Laszlo Vincze,[20] Joshua Von Korff,[1] Naomi Wordsworth,[36] Daniel Zevin,[1] Michael E. Zolensky,[14] 30714 Stardust@home dusters[37]

Seven particles captured by the Stardust Interstellar Dust Collector and returned to Earth for laboratory analysis have features consistent with an origin in the contemporary interstellar dust stream. More than 50 spacecraft debris particles were also identified. The interstellar dust candidates are readily distinguished from debris impacts on the basis of elemental composition and/or impact trajectory. The seven candidate interstellar particles are diverse in elemental composition, crystal structure, and size. The presence of crystalline grains and multiple iron-bearing phases, including sulfide, in some particles indicates that individual interstellar particles diverge from any one representative model of interstellar dust inferred from astronomical observations and theory.

Our understanding of the properties of contemporary interstellar dust (ISD) has been derived primarily from astronomical observations of the interstellar medium (ISM), including optical properties of the ISD and remote spectroscopy of the gas composition (*1*–*3*), and from in situ measurements by the dust analyzers on the Cassini, Ulysses, and Galileo spacecraft (*4*–*6*). The canonical picture of ISD is that it is dominated by ~0.2-μm-diameter (*7*) amorphous silicate grains, with or without carbonaceous mantles. However, the inferred properties of the particles, including size distribution, density, and composition, are heavily model dependent.

Direct, laboratory-based measurement of returned particles that may originate in the local ISM (LISM) offers an independent test of the assumptions on which the interpretation of spectroscopy and in situ dust measurements rest. Important questions to be addressed include: Is there one dominant dust phase, and if so, what is its composition? Is the dominant structure crystalline or amorphous? Is iron present in metal, oxide, carbide, and/or sulfide phases? Are the particles dense or fluffy? Is there evidence for particle mantles of either organic or silicate-like composition? We present here results from the Stardust Interstellar Preliminary Examination (ISPE) (*8*), in which we have identified seven dust particle impacts of probable interstellar origin, to address these and related questions. The identification of these seven impacts is the result of a massively distributed, volunteer-based, search of optical micrographs of the aerogel collectors, manual and automated searches of scanning electron micrographs of aluminum foils, extensive coordinated sample analyses, laboratory hypervelocity impact experiments, and numerical modeling of ISD propagation in the heliosphere. These are described in detail in a series of papers (*9*–*20*) published contemporaneously with this article; see also supplementary materials online (*21*).

The 0.1-m^2 Stardust Interstellar Dust Collector (SIDC) consisted of an Al frame holding ultralow-density silica aerogel tiles (*8*) that constitute 85% of the exposed area and Al foils that constitute the remaining 15%. The collector was exposed to the expected interstellar dust stream, approximately from the direction of Ophiuchus (*22*), for 195 days in two periods in 2000 and 2002. The low density of the silica aerogel enables capture of hypervelocity particles with mild deceleration as compared with other capture media, to limit the capture alteration effects, and simultaneously records particle trajectory in the form of a carrot-shaped track. The optical transparency of the aerogel allows for detection of tracks ≥2 μm in diameter (*9*). The Al foil is a collection medium that is complementary to the silica aerogel. Impact residues on the foils are localized to craters on the surface, which contain residue that is not mixed with silica aerogel. Scanning electron microscopy (SEM) of the foils can identify impact craters as small as 0.3 μm in diameter, corresponding to ~0.2-μm-diameter particles (*23*, *24*).

The criteria for identifying candidate interstellar particles (table S1) in the two collection media are slightly different. The first-order criteria (levels 0 to 2) are that the shape of the identified feature must be consistent with hypervelocity impact, and the captured particle or particle residue must have a composition that is consistent with formation in space, and inconsistent with spacecraft materials, or aerogel impurities. The trajectory of the particle is taken into consideration for the samples collected in aerogel, but not for the foils, because crater shapes depend strongly on the particle shape and composition, in addition to trajectory (*25*). The most definitive indication of an interstellar origin (level 3) for a particular particle would be an oxygen isotope composition inconsistent with solar system values. However, the converse is not true—an oxygen isotope composition within the range of solar system values does not uniquely constrain the origin to the solar system. All seven

[1]Space Sciences Laboratory, University of California at Berkeley, Berkeley, CA, USA. [2]Materials Science and Technology Division, Naval Research Laboratory, Washington, DC, USA. [3]Advanced Light Source, Lawrence Berkeley Laboratory, Berkeley, CA, USA. [4]Geoscience Institute, Goethe University Frankfurt, Frankfurt, Germany. [5]State University of New York at Plattsburgh, Plattsburgh, NY, USA. [6]Jacobs Technology/ESCG, NASA Johnson Space Center (JSC), Houston, TX, USA. [7]Institut für Geowissenschaften, University of Heidelberg, Germany. [8]Institut des Sciences de la Terre, Observatoire des Sciences de l'Univers de Grenoble, Grenoble, France. [9]Institut für Raumfahrtsysteme (IRS), University of Stuttgart, Stuttgart, Germany. [10]IGEP, TU Braunschweig, Braunschweig, Germany. [11]Max Planck Institut für Kernphysik, Heidelberg, Germany. [12]International Space Sciences Institute, Bern, Switzerland. [13]Carnegie Institution of Washington, Washington, DC, USA. [14]Astromaterials Research and Exploration Science, NASA JSC, Houston, TX, USA. [15]Field Museum of Natural History, Chicago, IL, USA. [16]Deutsches Elektronen-Synchrotron, Hamburg, Germany. [17]Space Research Centre, University of Leicester, Leicester, UK. [18]Department of Astronomy, University of Washington, Seattle, WA, USA. [19]University of Kent, Canterbury, Kent, UK. [20]University of Ghent, Ghent, Belgium. [21]University of New Mexico. [22]European Synchrotron Radiation Facility (ESRF), Grenoble, France. [23]University of Chicago, Chicago, IL, USA. [24]Washington University, St. Louis, MO, USA. [25]Max-Planck-Institut für Kernphysik, Heidelberg, Germany. [26]Max-Planck-Institut für Chemie, Mainz, Germany. [27]615 William Street, Apt 405, Midland, Ontario, Canada. [28]Natural History Museum, London, UK. [29]Advanced Photon Source, Argonne National Laboratory, Lemont, IL, USA. [30]Ecole Normale Superieure de Lyon, Lyon, France. [31]University Lille 1, France. [32]University of Hawai'i at Manoa, Honolulu, HI, USA. [33]NASA Ames Research Center, Moffett Field, CA, USA. [34]IRS, University Stuttgart, Stuttgart, Germany. [35]Jet Propulsion Laboratory, Pasadena, CA, USA. [36]Wexbury, Farthing Green Lane, Stoke Poges, South Buckinghamshire, UK. [37]Worldwide. List of individual dusters is at http://stardustathome.ssl.berkeley.edu/sciencedusters.
*Corresponding author. E-mail: westphal@ssl.berkeley.edu
†Deceased.

of the captured particles reported here are level 2 candidates, for which the oxygen isotope data are either not yet available, or are consistent with solar values. This means that although an interstellar origin cannot be definitively proven for the particles, other origins, including as interplanetary dust, have been determined to be statistically less likely than an interstellar origin. Three interstellar candidates were identified in a search of ~250 cm^2 of the exposed aerogel, and four interstellar candidates were identified in a search of ~5 cm^2 of the exposed Al foil.

Identification and analysis of candidates in aerogel

We identified 71 tracks in an examination of slightly over half of the aerogel tiles in the SIDC. All but two were identified through the Stardust@home project (*9*, *10*), in which volunteers searched online for tracks in digital micrographs of the aerogel collector. We extracted a subset of these tracks in volumes of aerogel, called "picokeystones" (*10*, *26*), and mounted them between 70-nm-thick Si_3N_4 membranes to protect from loss and contamination. Picokeystones were subsequently analyzed at one or more of six synchrotrons with techniques including scanning transmission x-ray microscopy (STXM) (*12*), Fourier transform infrared spectroscopy (FTIR) (*11*), x-ray fluorescence spectroscopy (XRF) (*13*–*15*), and x-ray diffraction (XRD) (*16*). Forty-six of the tracks are consistent in their trajectories with an origin as secondary ejecta from impacts on the aft solar panels, and this origin was confirmed for four tracks (*12*–*15*) by the presence of cerium, a cosmically rare element present in the glass covering the spacecraft solar panels. The remaining 25 so-called midnight tracks have trajectories that are consistent with an origin either in the interstellar dust stream or as ejecta from impacts on the lid of the sample return capsule (*20*). The ambiguity in origin of these 25 tracks is due to the articulation of the collector on its arm during the exposure (*27*). Because of the extremely limited amount of sample, we analyzed only the first 13 midnight tracks identified. Six showed aluminum x-ray absorption near-edge structure (XANES) spectra consistent with Al metal. These tracks are consistent with Al ejected from the sample return capsule by micrometeoroid impacts. Three tracks showed heavy-element abundances that pointed away from an extraterrestrial origin, and one could not be analyzed because of unusually high aerogel density. We focus here on three midnight tracks that are consistent with an extraterrestrial origin.

I1043,1,30,0,0 ("Orion") (Fig. 1) is a multicomponent, low-density particle compositionally consistent (see Table 1 for all particle characteristics) with a mixture of forsteritic olivine, magnesium-spinel, and iron-bearing phases with minor elements calcium, chromium, manganese, and nickel. Further composition details and discussion of errors are available (*21*). XRD and STXM analyses show a good fit to polycrystalline olivine, with mosaiced domains showing broadening in x-ray diffraction extending over 20°, nanocrystalline spinel, two undetermined crystalline phases of unknown composition, and an amorphous magnesium, aluminum oxide phase. One of the unidentified crystalline phases is consistent with iron metal nanoparticles. We derived an average density of ~0.7 g cm^{-3}. Elemental abundances normalized to magnesium and the composition of CI meteorites, whose abundances of nonvolatile elements are nearly identical to those of the Sun, and hence the bulk solar system, show 10-fold enrichments in aluminum and the minor element copper; depletions for silicon and calcium; and near normal iron, chromium, manganese, and nickel. Magnesium was used for normalization rather than the more usual silicon because its abundance could be measured precisely by STXM, whereas the silicon abundance is less certain owing to the silica aerogel background. Comparison of the Orion track morphology with hypervelocity analog shots (*17*) indicates a capture speed <10 km s^{-1}.

I1047,1,34,0,0: ("Hylabrook") (Fig. 2) is a magnesium-, iron-, and silicon-rich ~4-pg particle with a mosaiced, partially amorphized, forsteritic olivine core. This core is surrounded by a low-density halo, compositionally modeled as disordered magnesium-silicate, amorphous oxidized aluminum, amorphous metal oxides, and an iron-bearing phase, which may include reduced iron nanoparticles. The overall density of the particle (as captured) was ~0.3 g cm^{-3}. The major elements magnesium, silicon, and iron are present in CI-like relative proportions; magnesium-normalized elemental abundances show depletions in calcium and nickel, and enrichments in chromium, manganese, and copper, relative to CI. XRD data provide a good match to mosaiced olivine with an internal strain field up to 0.3%. The magnesium XANES spectrum shows that magnesium is present both in Hylabrook's crystalline core and in a partially amorphized olivine shell. The morphology of the track indicates that Hylabrook was also captured at <10 km s^{-1} (*17*).

Comparison of the morphology of track I1003,1,40,0,0 ("Sorok") with laboratory experiments (*17*) indicates that the capture speed was >15 km s^{-1} and that the original projectile had a mass of ~3 pg (Fig. 3). Silicon and carbon were detected in the track walls, but it is not clear whether the carbon is projectile residue, or carbon indigenous to the compressed aerogel, because carbon contamination is known to be present in the Stardust aerogel collectors (*28*). Organic materials are below detection limits in an FTIR analysis (*11*). Magnesium and aluminum were below detection limits in STXM analysis. If this particle had iron contents similar to those of Orion or Hylabrook and the entire particle residue were retained in the track, iron should have been detectable with STXM in the track walls. The nondetection of iron implies that either the original projectile was relatively iron-poor compared to Orion and Hylabrook, or that relatively little of the original projectile was retained in the track.

Identification and analysis of candidates on the aluminum foil

We identified 25 crater-like features after an automated SEM-based search of 13 individual Al foils (*19*). Elemental analysis, by either Auger electron spectroscopy or energy dispersive x-ray

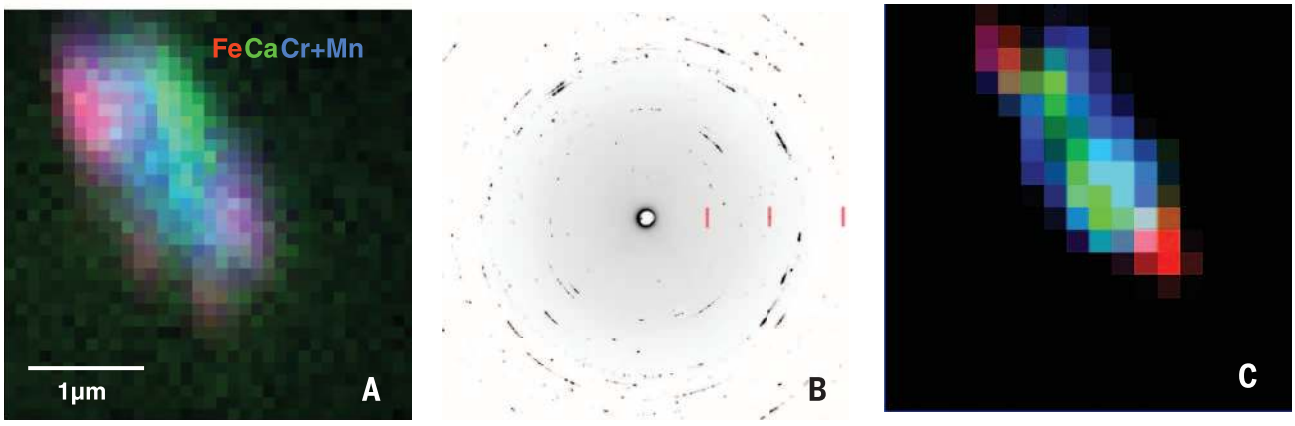

Fig. 1. Track I1043,1,30,0,0 ("Orion"). (**A**) Tri-color iron, calcium, (chromium+manganese) elemental map derived from XRF data. Colors are scaled to span the entire range of each element. (**B**) XRD pattern taken at 13.9 keV. Tick marks at d-spacings of 6, 3, and 2 Å are indicated. (**C**) Phase map. Colors indicate olivine (green), spinel (red), and an unidentified phase (blue).

spectroscopy (EDS), indicates that most of these features are impacts from fragments of the spacecraft solar panels. These craters contain residues rich in elements that are associated with the solar panel cover glass (boron, cerium, zinc, and titanium) and antireflection coating (fluorine), and that are of low cosmic abundance. Five of the features are associated with native defects in the foil and are not impact craters. Four of the impact craters contain residues with compositions inconsistent with spacecraft origin or native foil defects. The diameter of these candidate interstellar craters ranges from 0.28 to 0.46 μm. The crater diameter (D_c) is a function of particle diameter (D_p), capture speed, and density (*23*, *24*), with $D_c \sim 1.6D_p$ for silica spheres impacting Al_{1100} alloy at 6.1 km s^{-1}. Thus, the diameters of the particles that produced the craters range from ~0.2 to 0.3 μm. We extracted cross-sections of these craters with focused ion beam milling and then analyzed the cross-sections with scanning transmission electron microscopy (STEM) (*19*).

Dark-field STEM images and EDS maps (Fig. 4) of the cross-sections show the diversity of particle structure and composition. The residue in I1044N,3 is a silicate with a heterogeneous distribution of Mg, Si, and Fe, and no detectable sulfur. The residues in I1061N,3, I1061N,4, and I1061N,5 show both silicate and sulfide components. The shape of the crater provides an indication of the original distribution of the silicate and sulfide components, i.e, whether the impacting particle was a compact object with a single center of mass (1044N,3 and 1061N,3), or an aggregate with a few distinct centers of mass (I1061N,4 and I1061N,5). Quantitative individual element maps, including Ni, are shown in fig. S5.

Oxygen isotopic ratios were measured by secondary ion mass spectrometry on two of the crater cross-sections (*21*) and found to be consistent with solar system values within errors (Table 1). Oxygen isotope measurements of the two other craters were not possible owing to damage of the sections during transport between laboratories.

Low probability of an interplanetary origin

The combination of the elemental compositions of the seven ISD candidates with their impact feature characteristics (i.e., track shape and direction, or crater morphology) demonstrates that they are extraterrestrial in origin. However, further information is needed to distinguish between a possible interplanetary origin and an interstellar origin. The determination of origin cannot be based on elemental composition alone, because of the similarity of the solar nebula and the LISM in gas composition, and the overlap in range of temperature and pressure conditions at which dust condenses. The products of gas-solid condensation in each environment will share some common phases, including amorphous and crystalline silicates, oxides, and potentially also sulfides. For example, a ubiquitous component of primitive, probably cometary, interplanetary dust particles (IDPs) consists of GEMS (glass with embedded metal and sulfides) particles, which are similar to the canonical ISD particle in size, composition, and lack of crystallinity in the silicate phase and thus have been argued to be preserved interstellar particles (*29*). However, the origin of GEMS remains highly controversial (*30*). Only a small fraction of GEMS particles have oxygen isotopic anomalies proving an origin outside the solar system, but particles formed in the ISM at the time of solar birth could have had solar isotopic signatures.

Three of the four crater ISD candidates show elemental compositions within the range reported for GEMS, and two of these have solar-system–like oxygen isotopic ratios. The lack of strong oxygen isotopic anomalies rules out an origin in stellar outflows as inferred for meteoritic presolar grains. However, as with GEMS, normal oxygen isotopic composition does not preclude an origin in the ISM, because the range of isotopic compositions measured in the present-day ISM overlaps solar system values (fig. S5). The fourth, I1044N,3, has a lower silicon and higher oxygen content than GEMS and is thus more consistent with average values for the ISM dust composition (*2*). Orion and Hylabrook are distinct from GEMS in size, composition, and/or degree of crystallinity, but both are composed of phases previously observed in interplanetary and circumstellar particles: Orion contains olivine and spinel-like amorphous oxide; the magnesium-rich amorphous content of Hylabrook appears to be a rim on an interior olivine, rather than a distinct amorphous silicate.

Because of the ambiguity in distinguishing interstellar and interplanetary origins on the basis of chemical and isotopic compositions, stronger constraints on the particle origin(s) come from the geometry of the Stardust interstellar collection. Modeling indicates that very few IDP impacts on the SIDC are expected to coincide with the

Table 1. Summary of interstellar candidates.

ID	Mass or diameter	Composition	Structure	Capture speed (km s^{-1})
I1043,1,30,0,0 ("Orion")	3.1 ± 0.4 pg	Forsteritic olivine core (Mg_2SiO_4, 19 mol %), + nanocrystalline spinel + amorphous ($MgAl_2O_4$, 27 mol %) + Fe-bearing phase (47 mol %) with 7 mol % minor elements Cr, Mn, Ni, and Ca.	Low density (0.7 g cm^{-3})	<<10
I1047,1,34,0,0 ("Hylabrook")	4.0 ± 0.7 pg	Forsteritic ($Fo_{>80}$) olivine core (Mg_2SiO_4 30 mol %) surrounded by a low-density halo including amorphous Mg-silicate (1 mol %) + Al-, Cr-, Mn- (15 mol %), + Fe-bearing (54 mol %) phases.	Low density (<0.4 g cm^{-3})	<<10
I1003,1,40,0,0 ("Sorok")	~3 pg	Possible Si + C		> 15
I1044N,3	0.28-μm crater	Mg, Fe-rich silicate (Mg+Fe)/Si = 3.3	Single particle with chemical zoning	>10
I1061N,3	0.37-μm crater	Silicate (Mg:Fe:Si = 0.58:0.22:1 atomic %) + FeS $\delta^{17}O = -13 \pm 30$‰, $\delta^{18}O = 11 \pm 13$‰, $^{18}O/^{17}O = 5.36 \pm 0.18$ (1σ errors)	Single particle or nanoscale aggregate	~ 5 to 10
I1061N,4	0.39-μm crater	Silicate (Mg:Fe:Si = 0.33:0.15:1 atomic%) + Fe, Ni metal and sulfide	Two-particle aggregate with zoning of metal and sulfide	~ 5 to 10
I1061N,5	0.46-μm crater	Silicate (Mg:Fe:Si 0.57:0.15:1 atomic %) + Fe metal and Fe, Ni sulfide $\delta^{17}O = -85 \pm 61$‰, $\delta^{18}O = -20 \pm 27$‰, $^{18}O/^{17}O = 5.61 \pm 0.36$ (1σ errors)	Nanoparticle aggregate	~ 5 to 10

"midnight" direction where interstellar impacts occur (*10*, *19*), and we observed no tracks in the angular range where IDPs should have their maximum flux, indicating that the IDP background is small. Based on the observed angular distribution of captured particles, and model trajectories, the statistical likelihood of an interplanetary origin for all three interstellar dust candidates in aerogel is <0.03% (*10*, *20*). The ecliptic longitude of the interstellar dust radiant that best fits the observed trajectories of the three candidates in aerogel is somewhat larger than anticipated (*9*, *18*, *20*) based on observations from Ulysses and Galileo, but this may indicate a real long-term radiant shift, which is consistent with a long-term increase in radiant longitude in neutral helium, currently a topic of discussion (*22*, *31*).

Although the trajectories of the four foil interstellar candidates are unknown, statistical arguments based on trajectories still apply. We used the interplanetary micrometeoroid environment model (IMEM) (*21*, *32*) to estimate the fluence of IDPs >10^{-14} g collected to be 0.17 cm^{-2}. The observed impact density of nonterrestrial materials on the foils is 0.8 cm^{-2}, and thus the fraction of impacts of interplanetary origin is estimated to be 0.17/0.8 = 0.2. This value is in good agreement with the preflight estimates of Landgraf *et al.* (*33*), who predicted a total collected particle count of 120 (80 <2 μm and 40 >2 μm diameter) interstellar particles and 20 IDPs. With the conservative assumption that all of the interplanetary dust is <2 μm, this equates to 100 small particles (80 interstellar and 20 interplanetary), of which 20% should be interplanetary. Based on the good agreement of these two model calculations, we take 20% to be the probability of an interplanetary origin for any one impact, and <0.16% to be the probability that all four craters are interplanetary in origin. The latter estimate assumes an uncorrelated origin for the impacting particles. A correlated origin as secondary ejecta from micrometeroid impacts on the sample capsule or solar cell array can be discounted: In the ejecta of such impacts, spacecraft material is expected to dominate over impactor material by about two orders of magnitude (*9*, *20*) and to have lower impact velocity and shallower impact depth than should be observed for interstellar candidate craters (*34*). This is inconsistent with the observed low ratio of target/projectile material in the impacts, even accounting for the low statistics (*35*), and the observed interstellar candidate crater morphologies. A correlated origin as fragments of asteroidal or other collisional products can also be discounted. Such an origin would require a mechanism for maintaining correlated particle trajectories over large distances, against the differential solar light pressure and Lorentz forces that act on this size of particles. We conclude that an interstellar origin is most likely for the four candidate impact craters.

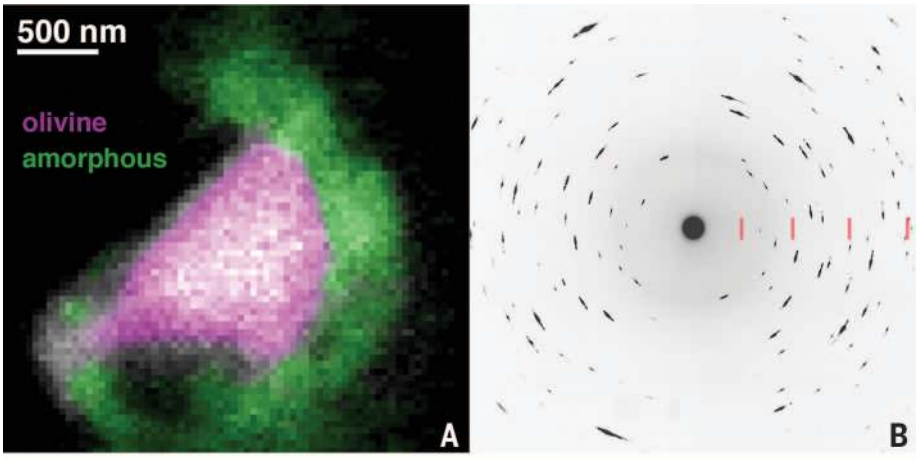

Fig. 2. Track I1047,1,34,0,0 ("Hylabrook"). (**A**) Bi-color olivine + amorphous phase map derived from STXM Mg XANES data. (**B**) XRD pattern taken at 13.9 keV. Tick marks at d-spacings of 6, 3, 2, and 1.55 Å are indicated.

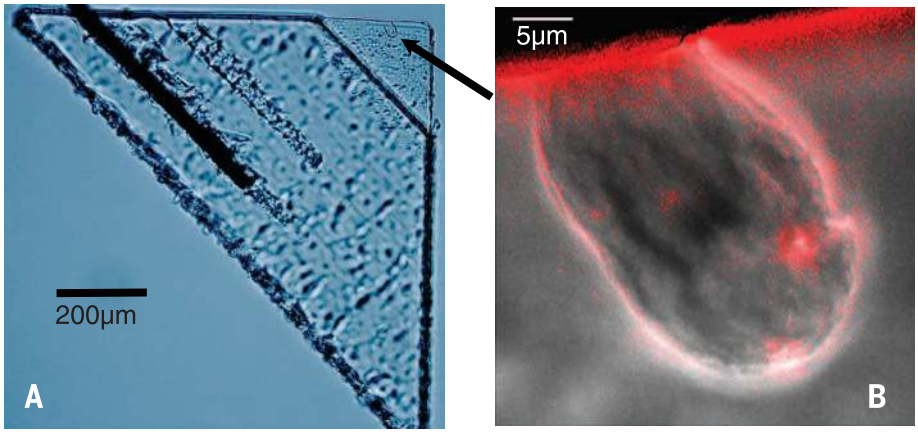

Fig. 3. Track I1003,1,40,0,0 ("Sorok"). (**A**) Optical micrograph of Sorok in its picokeystone. (**B**) STXM absorption map at 280 eV with overlaid map of carbon (red).

Implications for dust observations and modeling

Assuming that the captured particles are indeed all of interstellar origin, we can use their characteristics to address questions about the properties of contemporary interstellar dust. The particles in the aerogel and those in the foil represent two different size regimes. The particles captured in aerogel are >1 μm in diameter (~3 pg), which is consistent with the masswise dominant component of the dust sampled by in situ instruments on Ulysses and Galileo, but several hundred times more massive than the maximum dust size determined from observations of the ISM. The spectroscopic observations indicate a typical particle size of ~200 nm (~100 attograms for a density of ~2 g cm^{-3}). The particles captured in the Al foil are closer in size to that inferred for typical ISM particles by astronomical means. However, the in situ spacecraft data and models of heliospheric filtering (*18*) indicate that abundance of these particles is strongly reduced at 2 astronomical units compared to interstellar space than are the picogram-sized grains (*36*). Compared to the predictions prior to the Stardust sample return, we observed an order of magnitude fewer large particles (picogram-sized) and a factor of ~4 more small particles (attogram-sized) than expected from the in situ data.

The elemental compositions of the captured particles are generally consistent with expectations for ISD. Magnesium-rich silicates are common to all of the particles except Sorok, for which the actual particle composition could not be determined. In five of the particles (Orion, Hylabrook, and craters 1061N,3, 1061N,4, and 1061N,5), one or more distinct iron-rich phases were also observed. Some of the iron in Orion and Hylabrook may be in reduced form, and three of the particles captured in foil show FeS, and possibly metallic Fe. The chemical form of iron in ISD is uncertain. Estimates of the iron content of interstellar silicates vary widely [e.g., (*37*)], and the variation in Fe:Mg gas depletions in different regions of the ISM indicate that one or more iron-rich dust phases distinct from the magnesium-rich silicate are expected. The particular phase or phases are not known, because they do not provide distinct features in the ISM infrared (IR) spectra. Nanophase metallic Fe or FeS would be possible candidates, as both have broad, featureless IR spectra, and these phases are ubiquitous

components of primitive solar nebular materials and thus may also form as circumstellar and/or interstellar particles. The presence of a sulfide dust component in the ISM is a matter of debate. Most measurements of the ISM gas indicate little or no depletion of sulfur, compared to the solar abundance, which supports a lack of condensed sulfur-rich dust. However, uncertainty in determining the ISM gas-phase sulfur abundance and the difficulty of detecting nanophase sulfides with IR spectroscopy do not rule out the possibility that FeS nanoparticles are a component of ISM dust (*38*).

The crystallinity of the silicates in Orion and Hylabrook is unexpected. Spectroscopic measurements of interstellar silicates indicate that <2.2% are crystalline (*39*, *40*). Irradiation of the particles by gas accelerated by shockwaves in the diffuse intercloud medium are believed to effectively amorphize silicates in typical (~100 nm) ISD particles (*41*), but crystalline materials are probably preserved in the interiors of larger (>1 μm) particles. Crystalline silicates are observed in the outflows of oxygen-rich AGB stars (*42*) and observed as preserved presolar circumstellar particles in IDPs (*43*) and meteorites (*44*). Because the fraction of the mass contained in particles as large as Orion and Hylabrook (>3 pg) is <<1% of the condensed component of the ISM, the observation of crystalline material in them does not violate astronomical upper limits on silicate crystallinity (*39*, *40*). The mineralogical complexity of Orion may be consistent with assembly from small crystalline and amorphous components in a cold molecular cloud environment, whereas Hylabrook may be consistent with a single processed circumstellar condensate. This hypothesis may be testable by a future measurement of the isotopic composition of oxygen. The residues of the particles captured in the Al foil appear to be amorphous, but whether this is an original feature or an effect of hypervelocity capture alteration is unclear. Three of the four craters contain sulfides, whereas Orion contains only minor amounts of sulfur and Hylabrook has no appreciable sulfur content. This may be a further indication that larger particles sample a fundamentally different reservoir than small particles.

Optical and mechanical properties inferred from dust dynamics and statistics

Our measured fluence of >1-μm-diameter particles is ~1/10 of the prelaunch estimate (*33*). Because we used control images to measure detection efficiency in the Stardust collector, we can be confident that the difference is not due to detection inefficiency of high-speed impacts. However, the dynamics of nanometer- and micrometer-size particles in the heliosphere are strongly affected by radiation pressure exerted by sunlight. To investigate whether repulsion of interstellar dust by sunlight might play a role in reducing the flux in the inner solar system, we compared our observations of the track diameter distribution for our interstellar candidates with predictions of a model of interstellar dust propagation based on the Ulysses and Galileo (U/G) observations. We used a standard model of the optical properties of interstellar dust as a function of particle size (*4*) and the high-speed laboratory calibrations of interstellar dust analogs carried out as part of the present effort (*17*). We observed a markedly lower flux of high-speed interstellar dust than predicted by this model (Fig. 5), but a model developed as part of the ISPE (*18*) in which the optical cross section of the dust is larger and which takes into account Lorentz forces, is consistent with the observations. Further, the standard model predicted that nearly all impacts would be at high speed (>>10 km s^{-1}), because the model of optical properties assumed relatively compact, high-density dust particles. However, two of the three candidate impacts >1 μm were captured with speeds <<10 km s^{-1}. These observations can be most easily understood if interstellar dust in this size range consists of low-density material with a wide distribution of β, the ratio of radiation pressure force to gravitational force. Canonical ISD structures (*2*) consistent with such

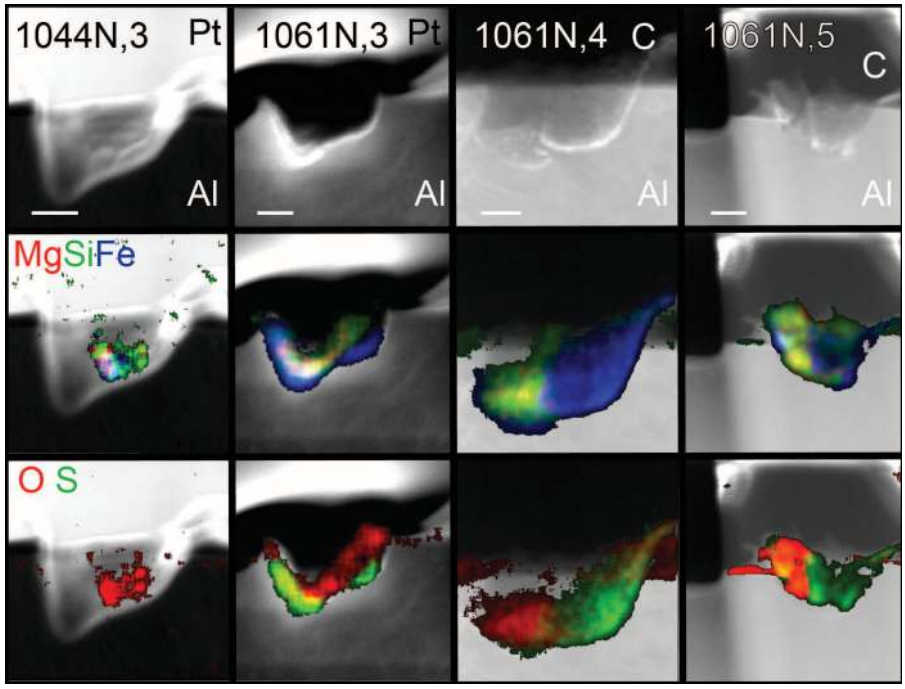

Fig. 4. Candidate interstellar dust impacts in Al foil. Dark-field STEM images (top row) and composite EDS element maps showing the Mg-Si-Fe and O-S distributions of the four candidate impacts. Pt and C refer to FIB-deposited protective masks. Scale bars: 100 nm.

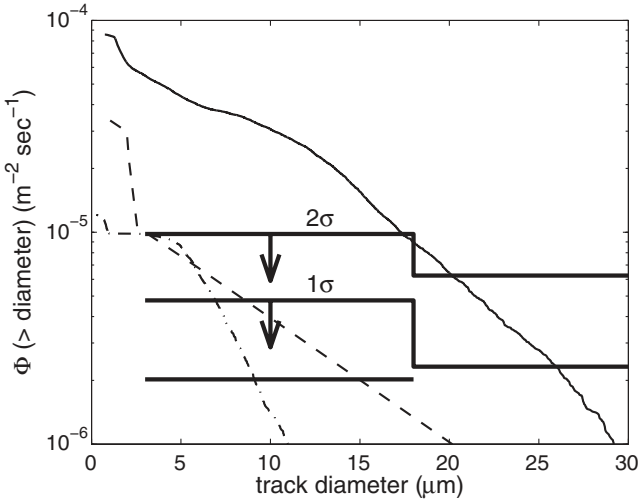

Fig. 5. Observed and predicted interstellar dust fluence. Comparison of the integral track areal density as a function of diameter observed in the Stardust aerogel collectors with the predictions of a model based on Ulysses and Galileo in situ observations (solid curve). The lower segment is the measured value, and stepped curves are 1σ and 2σ upper limits. For the prediction, we used an empirical model of track diameter versus particle diameter and capture speed derived from laboratory calibrations (*13*), and a standard model of β versus particle size (*4*). The dashed curve is a similar prediction based on work done under the ISPE (*18*), which includes a model of the optical properties of ISD with larger values of β, and includes Lorentz forces. The dot-dashed curve shows the same calculation, but with β taken to be three times the standard model of Landgraf *et al*. (*4*).

low-density particles include spheres with silicate cores and organic mantles, carbonaceous spheres, or aggregates of these. Of the seven candidate ISD particles, one is plausibly dominated by carbon and one is primarily a single silicate with a mantle-core structure, whereas the others are complex aggregates of various micrometer- to nanometer-size phases such as oxides, metal, and sulfides, in addition to silicate (Table 1).

The need for internal consistency leaves us with a twofold conclusion: If large interstellar dust particles consist of compact silicates with optical properties similar to those assumed by Landgraf *et al.* (*4*), then our results are in conflict with the U/G observations, and consistent with astronomical observations (*45*). By contrast, if large interstellar dust particles have low densities, which appears to be more likely based on trajectories, capture speeds, and compositions of our candidates, then our data can be consistent with the U/G observations, and possibly also with the astronomical observations, depending on the (currently unknown) wavelength dependence of the extinction cross sections of these particles. The latter conclusion is encouraging news for any future sample-return missions with the goal of capturing large numbers of relatively intact interstellar dust particles.

REFERENCES AND NOTES

1. P. C. Frisch, J. D. Slavin, *Earth Planets Space* **65**, 175–182 (2013).
2. H. Kimura, I. Mann, E. K. Jessberger, *Astrophys. J.* **583**, 314–321 (2003).
3. B. T. Draine, *Annu. Rev. Astron. Astrophys.* **41**, 241–289 (2003).
4. M. Landgraf, W. J. Baggaley, E. Grun, H. Kruger, G. Linkert, *J. Geophys. Res. Space Phys.* **105**, 10343–10352 (2000).
5. E. Grün *et al.*, *Nature* **362**, 428–430 (1993).
6. H. Krüger *et al.*, *Planet. Space Sci.* **58**, 951–964 (2010).
7. All particle sizes heareafter are given in diameter, rather than radius.
8. D. Brownlee *et al.*, *Science* **314**, 1711–1716 (2006).
9. A. J. Westphal *et al.*, *Meteorit. Planet. Sci.* 10.1111/maps.12168 (2014).
10. D. R. Frank *et al.*, *Meteorit. Planet. Sci.* 10.1111/maps.12147 (2014).
11. H. A. Bechtel *et al.*, *Meteorit. Planet. Sci.* 10.1111/maps.12125 (2014).
12. A. L. Butterworth *et al.*, *Meteorit. Planet. Sci.* 10.1111/maps.12220 (2014).
13. F. E. Brenker *et al.*, *Meteorit. Planet. Sci.* 10.1111/maps.12206 (2014).
14. A. S. Simionovici *et al.*, *Meteorit. Planet. Sci.* 10.1111/maps.12208 (2014).
15. G. J. Flynn *et al.*, *Meteorit. Planet. Sci.* 10.1111/maps.12144 (2014).
16. Z. Gainsforth *et al.*, *Meteorit. Planet. Sci.* 10.1111/maps.12148 (2014).
17. F. Postberg *et al.*, *Meteorit. Planet. Sci.* 10.1111/maps.12173 (2014).
18. V. J. Sterken *et al.*, *Meteorit. Planet. Sci.* 10.1111/maps.12219 (2014).
19. R. M. Stroud *et al.*, *Meteorit. Planet. Sci.* 10.1111/maps.12136 (2014).
20. A. J. Westphal *et al.*, *Meteorit. Planet. Sci.* 10.1111/maps.12221 (2014).
21. Supplementary details are available on *Science* Online.
22. R. Lallement, J. L. Bertaux, *Astron. Astrophys.* **565**, A41 (2014).
23. M. C. Price *et al.*, *Meteorit. Planet. Sci.* **45**, 1409–1428 (2010).
24. M. C. Price *et al.*, *Meteorit. Planet. Sci.* **47**, 684–695 (2012).
25. A. T. Kearsley *et al.*, *Meteorit. Planet. Sci.* **43**, 41–73 (2008).
26. A. J. Westphal *et al.*, *Meteorit. Planet. Sci.* **39**, 1375–1386 (2004).
27. P. Tsou, D. E. Brownlee, S. A. Sandford, F. Horz, M. E. Zolensky, *J. Geophys. Res. Planets* **108**, 8113 (2003).
28. S. A. Sandford *et al.*, *Meteorit. Planet. Sci.* **45**, 406–433 (2010).
29. J. P. Bradley, *Science* **265**, 925–929 (1994).
30. L. P. Keller, S. Messenger, *Geochim. Cosmochim. Acta* **75**, 5336–5365 (2011).
31. P. C. Frisch *et al.*, *Science* **341**, 1080–1082 (2013).
32. V. Dikarev, E. Grün, M. Landgraf, W. J. Baggaley, D. P. Galligan, in *Proceedings of the Meteoroids 2001 Conference*, B. Warmbein, Ed. (2001), vol. 495, pp. 609–615.
33. M. Landgraf, M. Müller, E. Grün, *Planet. Space Sci.* **47**, 1029–1050 (1999).
34. M. J. Burchell, M. J. Cole, M. C. Price, A. T. Kearsley, *Meteorit. Planet. Sci.* **47**, 671–683 (2012).
35. N. Gehrels, *Astrophys. J.* **303**, 336–346 (1986).
36. H. Krüger, E. Grün, *Space Sci. Rev.* **143**, 347–356 (2009).
37. M. Min, J. W. Hovenier, L. B. F. M. Waters, A. de Koter, *Astron. Astrophys.* **489**, 135–141 (2008).
38. E. B. Jenkins, *Astrophys. J.* **700**, 1299–1348 (2009).
39. F. Kemper, W. J. Vriend, A. G. G. M. Tielens, *Astrophys. J.* **609**, 826–837 (2004).
40. F. Kemper, W. J. Vriend, A. Tielens, *Astrophys. J.* **633**, 534–534 (2005).
41. A. P. Jones, J. A. Nuth III, *Astron. Astrophys.* **530**, A44 (2011).
42. F. J. Molster, L. Waters, *Astromineralogy* **609**, 121–170 (2003).
43. S. Messenger, L. P. Keller, D. S. Lauretta, *Science* **309**, 737–741 (2005).
44. C. Vollmer, P. Hoppe, F. E. Brenker, C. Holzapfel, *Astrophys. J.* **666**, L49–L52 (2007).
45. B. T. Draine, *Space Sci. Rev.* **143**, 333–345 (2009).

ACKNOWLEDGMENTS

We are deeply grateful to the Stardust@home dusters (list at http://stardustathome.ssl.berkeley.edu/sciencedusters), whose tremendous efforts were critically important to the success of this project. The ISPE consortium gratefully acknowledges the NASA Discovery Program for Stardust, the fourth NASA Discovery mission. NASA grants supported the following authors: NNX09AC36G—A.J.W., A.L.B., Z.G., R.L., D.Z., W.M., and J.V.K.; NNX09AC63G—C.F., R.D., A.L., W.J.O., K.S., and F.J.S.; NNH11AQ61I—R.M.S., H.C.G., and N.D.B.; NNX11AC21G—A.M.D., A.J.K., and T.S.; NNX11AE15G—G.J.F. The Advanced Light Source and the National Center for Electron Microscopy are supported by the Director, Office of Science, Office of Basic Energy Sciences, of the U.S. Department of Energy (DOE) under contract no. DE-AC02-05CH11231. Use of the National Synchrotron Light Source, Brookhaven National Laboratory, was supported by the U.S. DOE, Office of Science, Office of Basic Energy Sciences, under contract no. DE-AC02-98CH10886. Use of the Advanced Photon Source, an Office of Science User Facility operated for the U.S. DOE Office of Science by Argonne National Laboratory, was supported by the U.S. DOE under contract no. DE-AC02-06CH11357. M.T. and F.P. acknowledge support by Klaus Tschira foundation. A.A. and P.R.H. were supported by the Tawani Foundation. M.J.B. and M.C.P. are supported by Science and Technology Facilities Council (UK). F.E.B., J.K.H., P.H., J.L., F.P., S.S., R.S., and M.T. were supported by funding of the German Science Foundation (DFG) within SPP1385: the first ten million years of the solar system—a planetary materials approach. The ESRF ID13 measurements were performed in the framework of ESRF LTP EC337, with financial support by the Funds for Scientific Research (FWO), Flanders, Belgium (contract nr. G.0395.11, G.0257.12N and Big Science program G.0C12.13). G. Silversmit was postdoctoral fellow of the FWO during the ISPE investigations. Data presented in this paper are described in the supplementary materials and in references (*9*–*20*).

SUPPLEMENTARY MATERIALS

www.sciencemag.org/content/345/6198/786/suppl/DC1
Materials and Methods
Supplementary Text
Figs. S1 to S8
Tables S1 to S3
References (*46*–*56*)

21 February 2014; accepted 9 July 2014
10.1126/science.1252496

REPORTS

INTERSTELLAR MEDIUM

Pseudo–three-dimensional maps of the diffuse interstellar band at 862 nm

Janez Kos,[1]* Tomaž Zwitter,[1] Rosemary Wyse,[2] Olivier Bienaymé,[3] James Binney,[4] Joss Bland-Hawthorn,[5] Kenneth Freeman,[6] Brad K. Gibson,[7] Gerry Gilmore,[8] Eva K. Grebel,[9] Amina Helmi,[10] Georges Kordopatis,[8] Ulisse Munari,[11] Julio Navarro,[12] Quentin Parker,[13,14,15] Warren A. Reid,[13,14] George Seabroke,[16] Sanjib Sharma,[5] Arnaud Siebert,[3] Alessandro Siviero,[17,18] Matthias Steinmetz,[18] Fred G. Watson,[15] Mary E. K. Williams[18]

The diffuse interstellar bands (DIBs) are absorption lines observed in visual and near-infrared spectra of stars. Understanding their origin in the interstellar medium is one of the oldest problems in astronomical spectroscopy, as DIBs have been known since 1922. In a completely new approach to understanding DIBs, we combined information from nearly 500,000 stellar spectra obtained by the massive spectroscopic survey RAVE (Radial Velocity Experiment) to produce the first pseudo–three-dimensional map of the strength of the DIB at 8620 angstroms covering the nearest 3 kiloparsecs from the Sun, and show that it follows our independently constructed spatial distribution of extinction by interstellar dust along the Galactic plane. Despite having a similar distribution in the Galactic plane, the DIB 8620 carrier has a significantly larger vertical scale height than the dust. Even if one DIB may not represent the general DIB population, our observations outline the future direction of DIB research.

Diffuse instellar bands (DIBs) are wide and sometimes structured absorption lines in the optical and near-infrared (NIR) wavelengths that originate in the interstellar medium (ISM) and were discovered in 1922 (*1*, *2*); more than 400 are known today (*3*), but their physical carriers are still unidentified (*4*–*8*). Their abundances are correlated with interstellar extinction and with abundances of some simple molecules (*9*), so DIBs are probably

www.sciencemag.org/345/6198/786/suppl/DC1

Supplementary Materials for

Evidence for interstellar origin of seven dust particles collected by the Stardust spacecraft

Andrew J. Westphal,* Rhonda M. Stroud, Hans A. Bechtel, Frank E. Brenker, Anna L. Butterworth, George J. Flynn, David R. Frank, Zack Gainsforth, Jon K. Hillier, Frank Postberg, Alexandre S. Simionovici, Veerle J. Sterken, Larry R. Nittler, Carlton Allen, David Anderson, Asna Ansari, Saša Bajt, Ron K. Bastien, Nabil Bassim, John Bridges, Donald E. Brownlee, Mark Burchell, Manfred Burghammer, Hitesh Changela, Peter Cloetens, Andrew M. Davis, Ryan Doll, Christine Floss, Eberhard Grün, Philipp R. Heck, Peter Hoppe, Bruce Hudson, Joachim Huth, Anton Kearsley, Ashley J. King, Barry Lai, Jan Leitner, Laurence Lemelle, Ariel Leonard, Hugues Leroux, Robert Lettieri, William Marchant, Ryan Ogliore, Wei Jia Ong, Mark C. Price, Scott A. Sandford, Juan-Angel Sans Tresseras, Sylvia Schmitz, Tom Schoonjans, Kate Schreiber, Geert Silversmit, Vicente A. Solé, Ralf Srama, Frank Stadermann, Thomas Stephan, Julien Stodolna, Stephen Sutton, Mario Trieloff, Peter Tsou, Tolek Tyliszczak, Bart Vekemans, Laszlo Vincze, Joshua Von Korff, Naomi Wordsworth, Daniel Zevin, Michael E. Zolensky, 30714 Stardust@home dusters

*Corresponding author. E-mail: westphal@ssl.berkeley.edu

Published 15 August 2014, *Science* **345**, 786 (2014)
DOI: 10.1126/science.1252496

This PDF file includes:

Materials and Methods

The methods and measurements are described in detail in the series of supporting papers published contemporaneously with this article (*9-20*).

Table S1. Criteria for Classification of Captured Candidate Interstellar Particles.

	Aerogel	Al Foil
Level 0	Impact-like feature in aerogel	Impact-like feature in the foil
Level 1	Track or impact feature definitively confirmed by high-resolution optical microscopy	Impact crater confirmed by scanning electron microscopy
Level 2	Trajectory consistent with interstellar origin and composition inconsistent with spacecraft materials	Residue composition inconsistent with spacecraft materials
Level 3	O isotope composition inconsistent with solar values	O isotope composition inconsistent with solar values

Supplementary Text

1. Backgrounds

The two sources of background in the search for interstellar dust particles are interplanetary dust particles and particles in the secondary ejecta from micrometeoroid impacts on the spacecraft that are dominated by extraterrestrial projectile material. We have presented assessments of both background sources in (*10*), but expand on them here.

To assess the probability that the three interstellar candidates in aerogel have an interplanetary rather than interstellar origin, we used our observation of zero interplanetary dust particles in the range of azimuth angles that mostly excludes secondary ejecta from impacts on the SRC deck or on the solar panels. We test the hypothesis that three interplanetary dust particles, following the distribution shown in Fig. 2 of Frank et al. *(10),* would fall into the azimuth range consistent with an origin in the interstellar dust stream. Using a Monte Carlo simulation, we find that this probability is less than ~3×10^{-4}. Distributions for inclination and eccentricity for the Monte Carlo simulation of IDP trajectories were taken from the model of Nesvorny (*46*). Semi-minor axes were not given in that paper, but we found that the results were insensitive to the distribution of semi-minor axis. In Fig. 2 of Frank et al. (*10*) we assumed a uniform distribution of semi-major axis from 3 AU to 9 AU. We assumed an equal probability of

capture for each of the 195 days of the exposure, and an equal probability of capture for inbound or outbound sections of the orbit. We also note that the 99% of the interplanetary micrometeoroids observed in the Monte Carlo simulation were captured at speeds > 7.5 km sec^{-1}, which appears to be inconsistent with the low capture speeds of Orion and Hylabrook.

Asteroidal dust is a possible source of background in the identification of interstellar dust. Nesvorny et al. (*46*) found that the fraction of interplanetary dust that has an asteroidal origin is <15% within 10º of the ecliptic, and that most interplanetary dust has a cometary origin, which we modeled by Monte Carlo (Fig. 2 of Frank et al.). Thus, our upper limit on interplanetary cometary dust gives an even stricter upper limit on asteroidal dust, by at least a factor of six.

To investigate this possibility further, we performed Monte Carlo simulations of capture trajectories of asteroidal dust in the collector. The two largest populations of asteroidal dust are the Karin and Veritas populations (*47*). We used the approximate distributions of eccentricity, semi-major axis and inclination for these two populations given by Nesvorny et al. (*47*). In both cases, all 10,000 simulations of particle trajectories appeared at azimuths far from those of the three candidates in aerogel, and in the opposite hemisphere of the sky (Figs. S1 and S2). Simulations of dust impacts from rare, so-called main-belt comets (Jewitt et al.) (*48*), Hsieh et al. (*49*)) give similar results. We also carried out a Monte Carlo simulation of the impact directions of hypothetical particles ejected from 1087 Main Belt asteroids, taken from the SKADS catalog (*50*). The trajectories are shown in Fig. S3. 2.0% of the simulations fall in the azimuth range consistent with the three candidates in aerogel, so the probability that all three candidates in aerogel are drawn from this distribution is 8×10^{-6}. Azimuth angle measurements were conducted on the particle tracks before extraction of the tracks from the aerogel tiles, and before extraction of the tiles from the tray. We monitored changes in zenith angle during tile or picokeystone extraction using fixed artificial reference tracks in the same picokeystones. In all cases errors in trajectory measurements were negligible compared with spacecraft wobble.

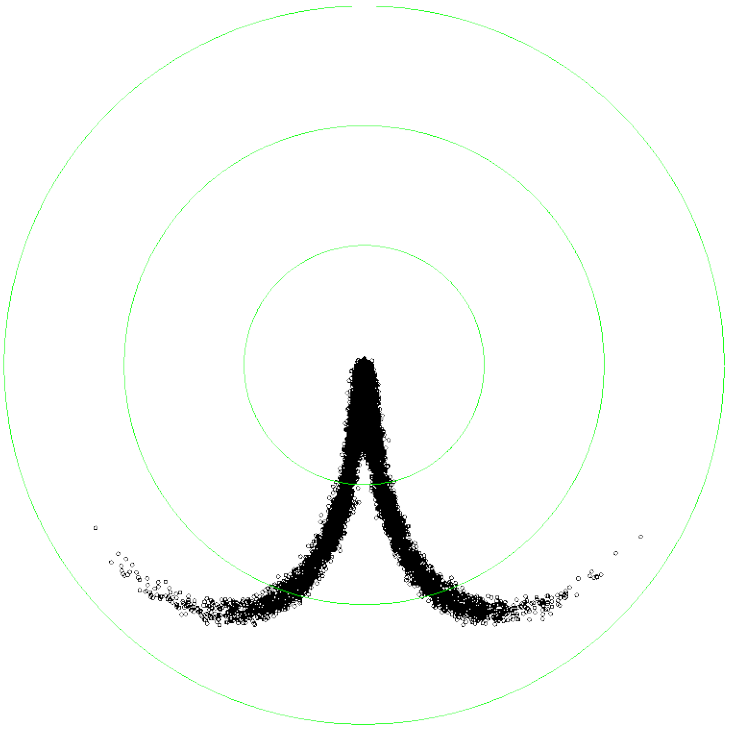

Fig. S1. Monte Carlo simulations of the trajectories of asteroidal particles from the Karin population. The coordinate system is identical to Fig. 2 of Frank et al. (*10*): The green contours are at 30º, 60º and 90º; the sunward direction is up.

Fig. S2. Monte Carlo simulations of the trajectories of asteroidal particles from the Veritas population. The coordinate system is identical to Fig. 2 of Frank et al. (*10*): The green contours are at 30º, 60º and 90º; the sunward direction is up.

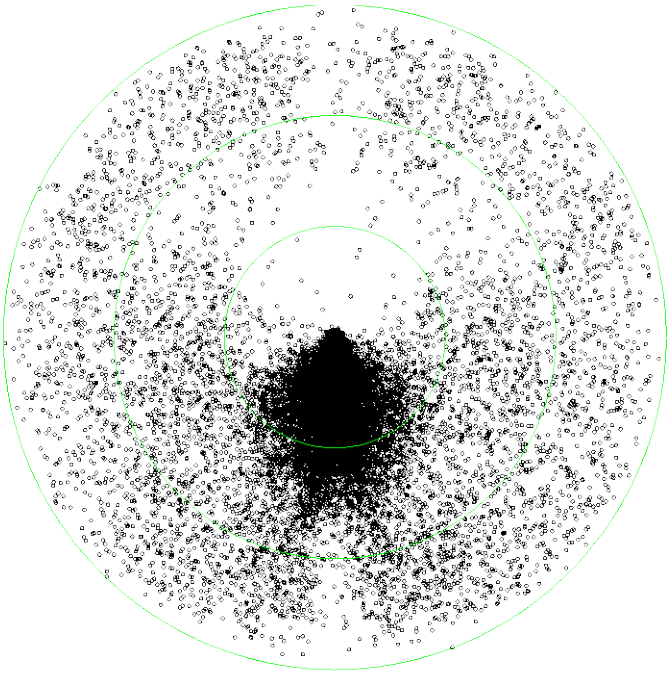

Fig. S3. Monte Carlo simulations of the trajectories of hypothetical asteroidal particles released from 1087 Main Belt asteroids, taken from the SKADS catalog (*50*). The coordinate system is identical to Fig. 2 of Frank et al. (*10*): The green contours are at 30º, 60º and 90º; the sunward direction is up.

In the assessment of the background due to secondary ejecta in (*10*), we assumed an asymptotically large exposure factor on the spacecraft, so that the entire interplanetary dust spectrum was sampled. The probability distribution of the target/projectile (T/P) ratio in the ejecta is a strong function of interplanetary dust fluence: for small fluences, ejecta from impacts of small projectiles dominate, so a small T/P ratio is most likely, while for sufficiently large exposures, ejecta from relatively rare large projectiles dominate, resulting in large T/P ratios as the most probable. Here we calculate the statistical likelihood that the interstellar dust candidates consist of secondary particles, using an estimate of the finite fluence of interplanetary dust particles on the spacecraft.

The Interplanetary Micrometeoroid Environment Model (IMEM) code is a tool that predicts micrometeoroid fluence with a defined size range, on a surface with a defined orientation, over a defined segment of a Keplerian orbit (*32*). We used IMEM to calculate the fluence of micrometeoroids on the deck of the Stardust Sample Return Capsule for the two collection periods. The result was 116 impacts greater than 1 pg. We scaled this result to that of the Grün model (*51*) for a rotating flat plate at 1AU, which gives 263 such impacts. Thus the SRC deck would have received about 44% of the nominal fluence predicted by the Grün model. IMEM also predicted an average impact speed of ~10 km s^{-1} , instead of 12 km s^{-1} in our simulation based on Nesvorny et al. (*47*). We thus assumed 10 km s^{-1} average impact speed in subsequent calculations because it tends to give a lower target/projectile ratio, which is the more conservative assumption. We

then used a Monte Carlo simulation to calculate the median and 2σ lower limits on the T/P mass ratio in the ejecta, as a function of micrometeoroid fluence, normalized to the prediction of the Grün model. To compute the T/P ratio for each projectile in the Monte Carlo simulation, we used the observations of crater diameters in aluminum targets as a function of projectile size, reported by Price et al. (*23*). We assumed that the amount of ejected target material was proportional to the crater volume, and we assumed that the target material and projectile material were ejected from the impact with equal efficiency. We then compared this to the 2-σ upper limit on the target/projectile ratio for tracks in aerogel and craters in foils. Fig. S4 shows the result. The solid line is the median T/P ratio as a function of micrometeoroid fluence, in units of the Grün model prediction, the dashed line is the 2σ lower limit, and the solid blue and red lines are the 2σ upper limits from the track and crater statistics. The green line is the IMEM prediction. We conclude that the actual micrometeoroid fluence is a factor of two greater than the maximum fluence on the SRC that gives consistency at the ≤3σ level in the T/P ratio between the Monte Carlo simulation and the observations in the aerogel. Since the solar panels are so much larger than the SRC, this factor is even greater for the craters. We conclude that the observed T/P ratio is inconsistent with a secondary origin for the interstellar candidates in either aerogel or foils.

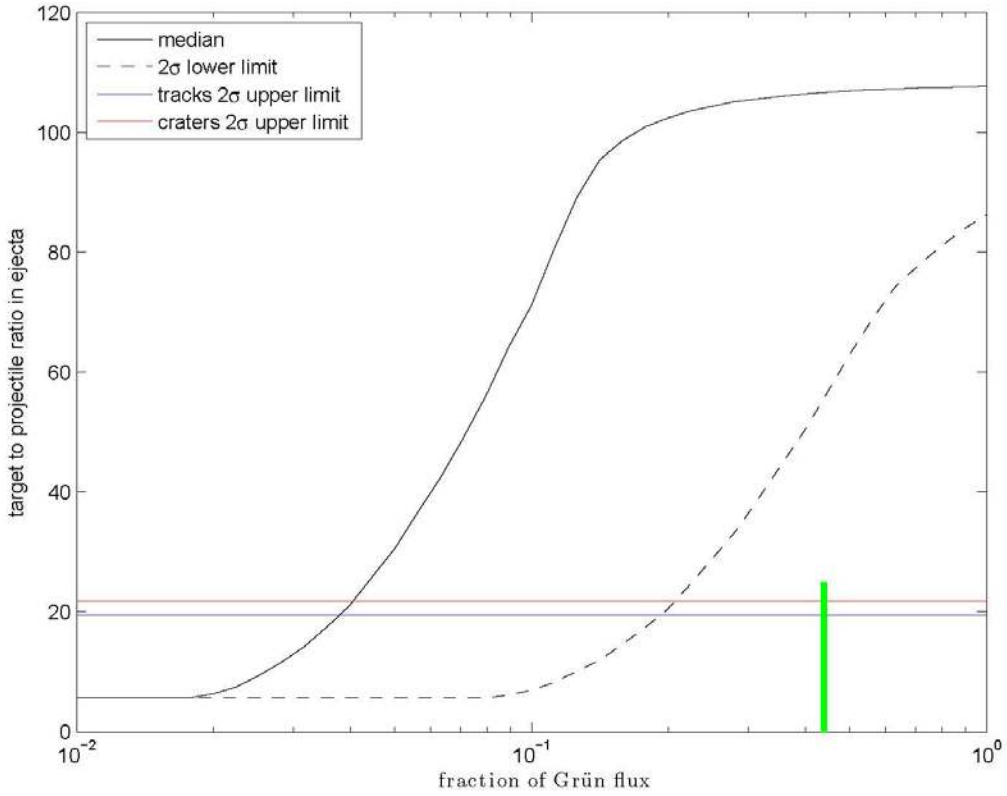

Fig. S4. Monte Carlo simulations of the target/projectile mass ratio in the ejecta of micrometeoroid impacts on the Stardust Sample Return Capsule deck, as a function of micrometeoroid fluence, normalized to the prediction of the Grün model for particles > 10 μm. The green line indicates the fluence received by Stardust as predicted by IMEM.

We also explored the possibility that the ejection of target material was suppressed relative to the projectile material for small projectiles. For projectiles larger than 10µm in diameter, cratering seems to be self-similar on all scales, but self-similarity breaks down for polycrystalline Al targets and projectiles near to or smaller than the Al crystallite grain size. Because we have no experimental information about the relative ejection rates of target and projectile material, we took a conservative approach, and assumed that below 10µm, no target material is ejected, and all the projectile material is ejected. Fig. S5 shows the result. Although the curve shows the effects of this assumption at low fluence, there is no change in the general conclusion.

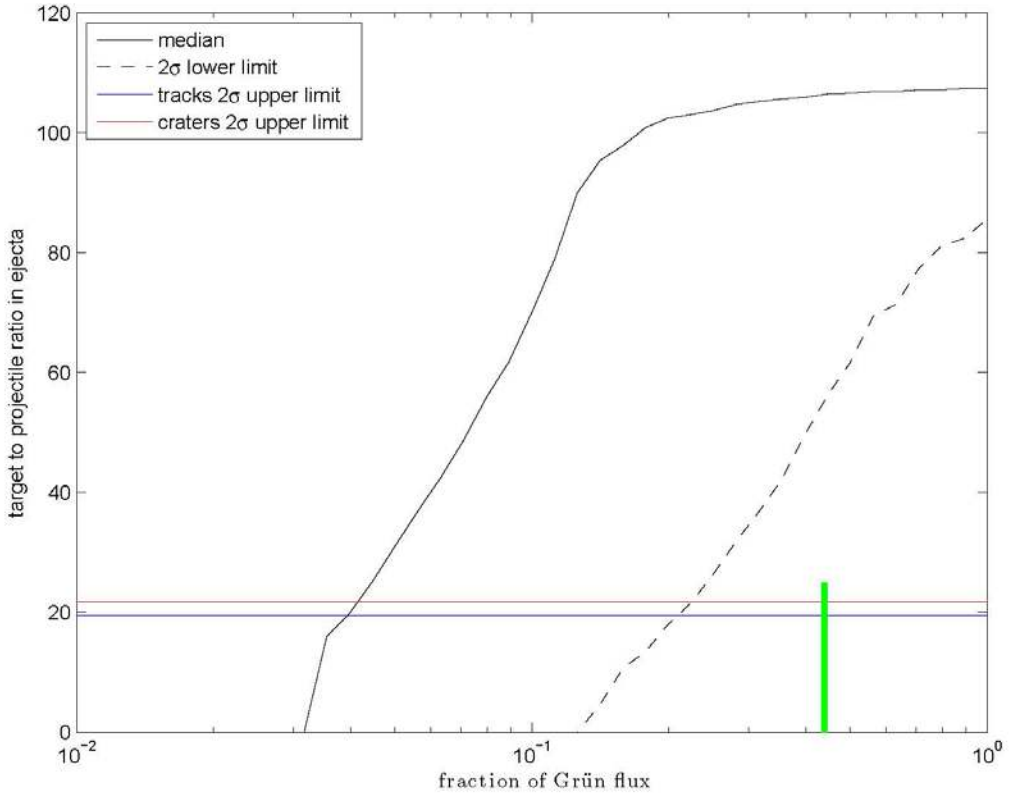

Fig. S5. Monte Carlo simulations of the target/projectile mass ratio in the ejecta of micrometeoroid impacts on the Stardust Sample Return Capsule deck, as a function of micrometeoroid fluence, normalized to the prediction of the Grün model (*51*) for particles > 10 µm. The green line indicates the fluence received by Stardust as predicted by IMEM. Here we assume that no target material is ejected for impacts of projectiles < 10 µm in diameter.

2. STEM analyses of crater residues

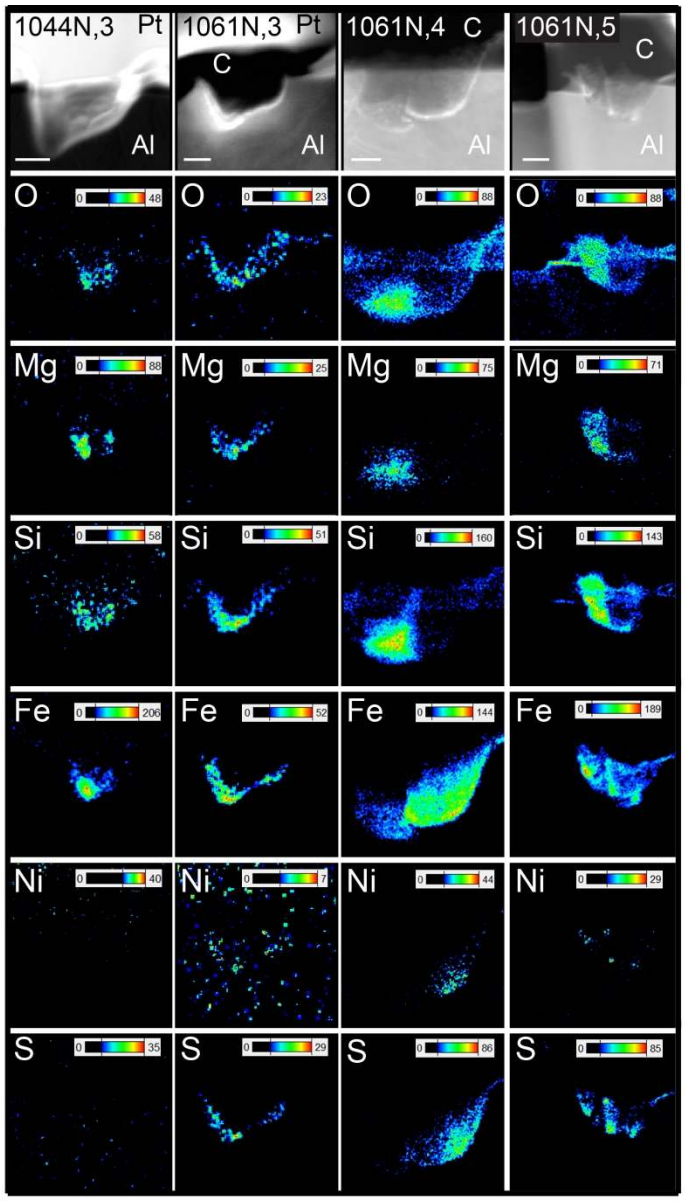

Fig. S6. Dark field STEM images (top row) and net-count EDS element maps of the four candidate interstellar dust impact residues in Al foil. Scale bars indicate 100 nm. Pt and C refer to FIB-deposited protective masks.

Figure S6 shows the spatial distribution of the elemental components in the impact crater residues, extracted from STEM-EDS spectrum images. 1044N,3 shows clear zoning of the Mg, Si and Fe contents, but is a single particle. 10661N,3 shows mixed silicate and sulfide components, indicating a single particle or fine-grained aggegrate. 1061N,4 shows zoning into two components > 100 nm, one silicate and one sulfide, consistent with the

double-bowl shape of the crater that indicates two mass centers. 1061N,5 also shows distinct silicate and sulfide components, but the Ni and S distribution indicate that the sulfide consisted of multiple particles < 10 nm.

3. Crater oxygen isotope measurements

We used secondary ion mass spectrometry to measure O isotopes on Focused-Ion Beam (FIB) cross-sections of two candidate interstellar impact craters, one crater found to contain residue from solar panel cover glass, and two similarly sized impact craters from the Stardust Wild 2 cometary Al-foil collection (*19*). In order to minimize instrumental artifacts associated with measurements of cross-sections suspended on Omniprobe grids, the crater FIB sections were first removed from TEM Omniprobe grids, transferred to clean Au foils and coated with a thin Au coat as described in (*19*). Analyses were carried out with a Cameca NanoSIMS 50L ion microprobe at the Carnegie Institution of Washington. A <1 pA, ~100 nm diameter Cs^+ primary ion beam was rastered (128×128 pixel, 16–25μm^2) over each sample and negative secondary ions of $^{12,13}C$, $^{16,17,18}O$, ^{28}Si, and $^{27}Al^{16}O$ were simultaneously collected along with secondary electrons in multicollection imaging mode, with total dwell times of ~0.25 seconds per pixel. The cometary craters, solar cell glass crater and contamination present in all samples were used to correct for instrumental mass fractionation and possible different detection efficiencies of the electron multipliers used to detect the secondary ions. Isotopic images were quantitatively analyzed with the L'image software (L. Nittler, CIW). Errors are completely dominated by counting statistics. Figure S7 shows NanoSIMS images for the two interstellar candidate craters; crater residue is clearly resolvable.

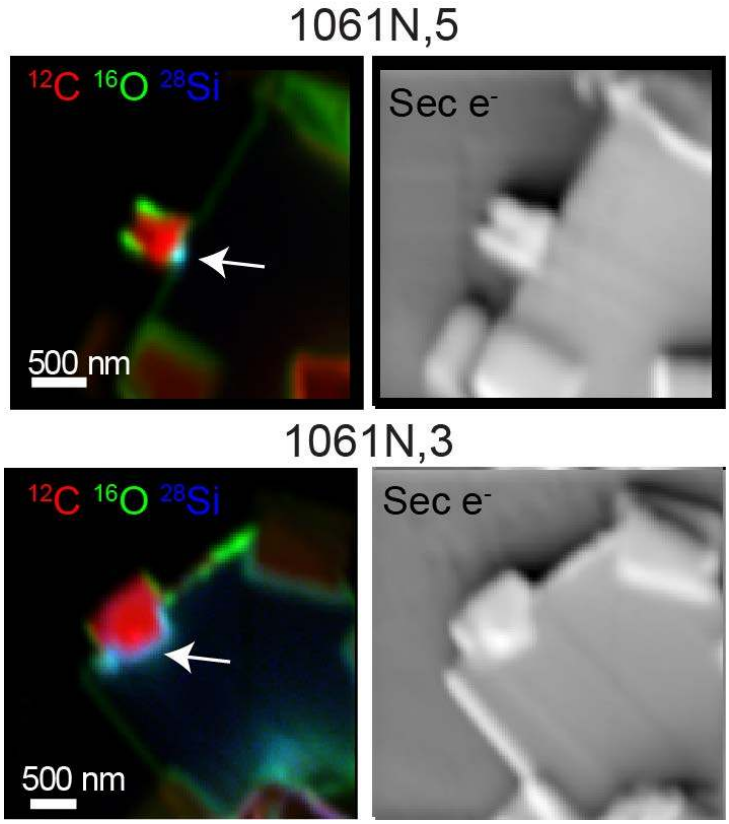

Fig. S7. NanoSIMS images of two interstellar candidate crater FIB cross-sections. Left panels indicate red-green-blue overlays of signals from ^{12}C, ^{16}O, and ^{28}Si, respectively, while right panels show the corresponding secondary electron images. Arrows indicate crater residues.

Derived oxygen isotope ratios are shown in Figures S8 and S9. The interstellar candidate residues have oxygen isotope ratios indistinguishable from those of the cometary and solar panel glass residues and contamination on the samples. O-rich presolar circumstellar grains in meteorites and comet samples have very large O-isotopic anomalies [e.g. refs *30*, *43*, *44*] such that they typically plot outside of the range of Fig S8. The measured compositions for the residues hence are clearly incompatible with a stellar origin. However, even grains formed in the ISM may have non-solar O isotopic ratios. For example, radio telescopic measurements of molecular clouds throughout the Galaxy have revealed them to typically have lower $^{18}O/^{17}O$ ratios (~4.1) than the Solar System value of 5.2 (Figs. S8 and S9). Recent infrared measurements of a few young stellar objects have found similar non-solar $^{18}O/^{17}O$ ratios (*52*). The origin of the oxygen isotopic discrepancy between much of the present-day Milky Way interstellar medium and the Solar System is controversial, and both supernova injection into the Sun's parental molecular cloud (*53*) and the chemical evolution of the Galaxy in the 4.6 Ga since solar birth (*54*) have been proposed. The interstellar observations would seem to indicate that interstellar dust forming today in the ISM should have lower-than-solar $^{18}O/^{17}O$ ratios on average, in contrast with our two candidate crater measurements. However, the molecular cloud observations show considerable scatter, for example one

cloud at the Sun's galactocentric radius is seen to have a solar-like $^{18}O/^{17}O$ ratio (arrow, Fig. S9). The oxygen isotopic composition of the local ISM from which our candidate particles may have originated has not been directly measured, and it is thus possible that it has a solar-like composition. The normal oxygen isotopic composition measured in the two crater residues therefore does not rule out an interstellar origin.

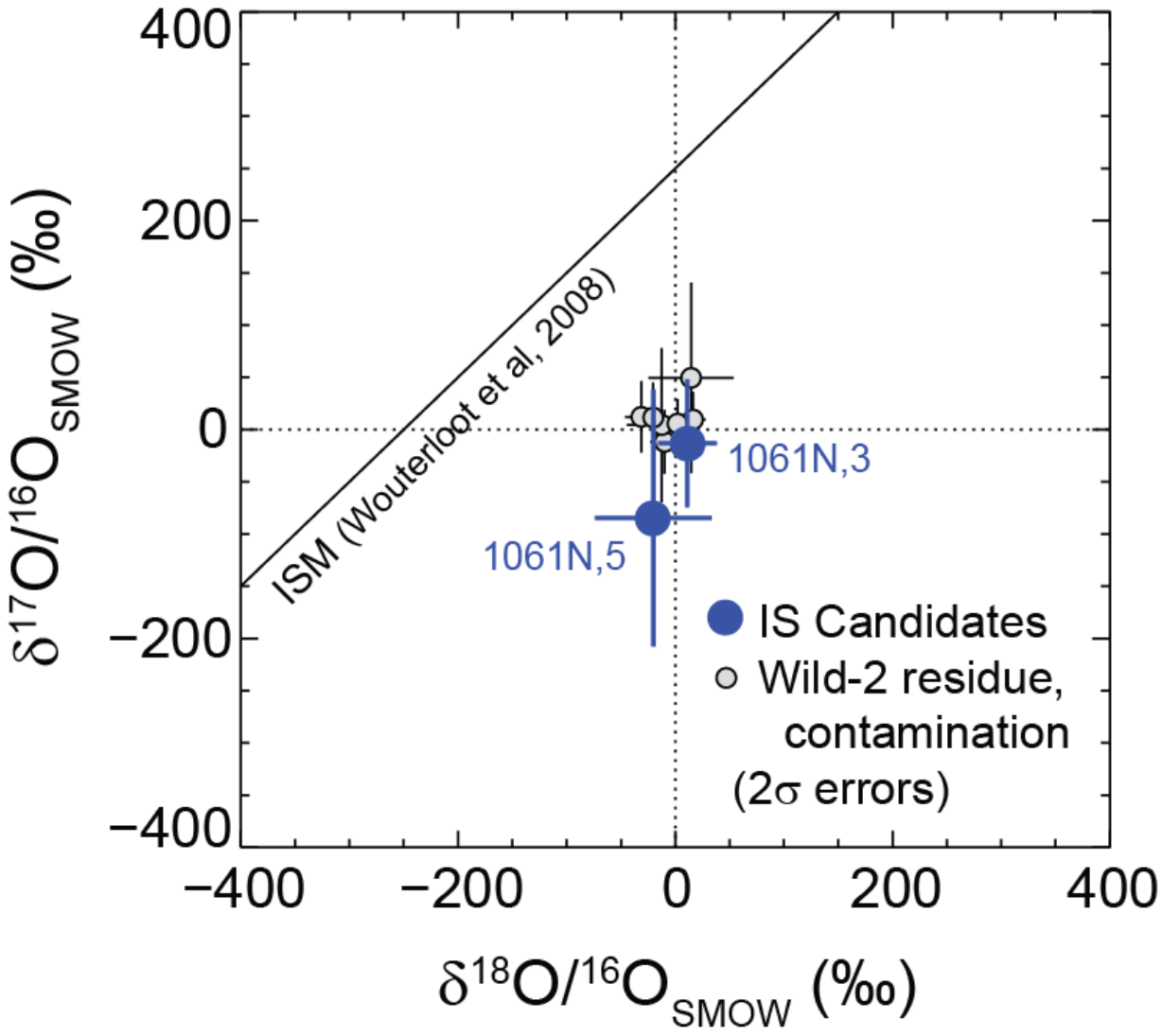

Fig. S8. Oxygen 3-isotope plot for candidate interstellar crater residues and other measured samples. Isotopic ratios are given as delta-values, ‰ deviations from Standard Mean Ocean Water (SMOW), represented by dotted lines. All measured values are within errors of terrestrial and distinct from the average composition of molecular clouds as determined by astronomical observations (*55*).

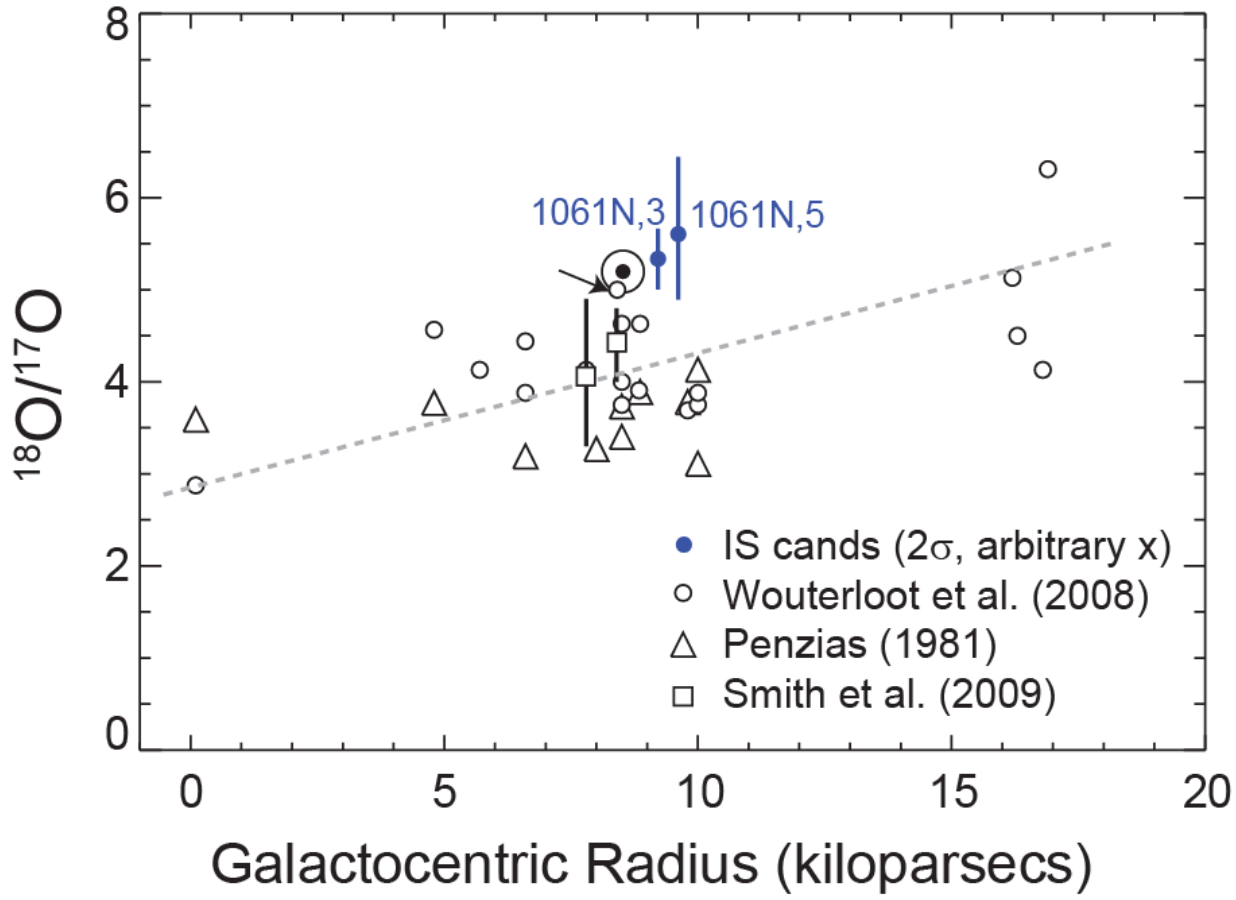

Fig. S9. $^{18}O/^{17}O$ ratios of two interstellar candidate crater residues (blue symbols, plotted at arbitrary abscissa values) are compared to astronomical measurements of molecular clouds (open circles and triangles, (*56*) and (*55*)) and young stellar objects (squares, (*52*)). Dashed line indicates possible galactic gradient in $^{18}O/^{17}O$ ratio suggested by Wouterloot et al. data (*55*). Arrow indicates one molecular cloud with solar-like $^{18}O/^{17}O$ ratio. After Nittler and Gaidos (*54*).

3. Composition of Orion

The oxidation state of Fe in Orion is unknown, resulting in an uncertainty in stoichiometric oxygen, hence there are uncertainties in the bulk atomic fractions and total mass of the particle (Table S.2) and in estimation of the fraction of Orion's molecular phases (Table S.3). We assumed stoichiometric forsteritic olivine (Mg_2SiO_4), spinel ($MgAl_2O_4$) and S occurred as FeS, but we do not imply that these phases were present as crystalline minerals in Orion. Based on XRD evidence that one Fe phase is consistent with Fe nanoparticles, we favor the assumption that the major Fe phase is Fe/FeO (some mix of Fe^0 and Fe^{2+}). The major phase composition is thus: Mg_2SiO_4 19.2±3.3 mol%, $MgAl_2O_4$ 27.5±2.3 mol% and Fe/FeO 44.7±3.5 mol%. In Table S.3 we show the effect on the bulk molecular fractions if the non-sulfide Fe was completely oxidized to Fe_2O_3.

Table S2. Elemental composition of Orion depending on Fe oxidation state.

Element	Measured Mass femtogram	Atomic Fraction Reduced Fe	Atomic Fraction (FeO) Fe^{2+}	Atomic Fraction (Fe_2O_3) Fe^{3+}
Mg (olivine)	300 ±60	10.1±2.0 %	8.9±1.8 %	8.5 %
Mg (spinel)	200 ±40	6.7±1.3 %	6.0±1.2 %	5.7 %
Al	475 ±35	14.3±1.1 %	12.7±0.9 %	12.1 %
Fe	840 ±100	12.3±1.5 %	10.9±1.3 %	10.3 %
S	23 ±10%	0.6±0.12 %	0.5±0.1 %	0.5 %
Ca	23 ±10%	0.5±0.05 %	0.4±0.04 %	0.4 %
Cr	12 ±10%	0.2±0.02 %	0.2±0.02 %	0.2 %
Mn	14 ±10%	0.2 ±0.02 %	0.2±0.02 %	0.2 %
Ni	55 ±10%	0.08±0.08 %	0.7±0.07 %	0.6 %
Cu	11 ±10%	0.1±0.01 %	0.1±0.01 %	0.1 %
Si*		*5.0 %*	*4.5 %*	*4.2 %*
O*		*49.3 %*	*54.9 %*	*57.2 %*
Total Particle Mass		3.1 pg	3.3 pg	3.4 pg

* Si and O are assigned stoichiometrically without implying that phases are crystalline.

Table S3. Bulk molecular phases in Orion, varying the unknown Fe phase.

Phase	Molar fraction Fe metal	Molar fraction FeO	Molar fraction Fe_2O_3
Forsterite (Mg_2SiO_4)	19.2±3.3 %	19.2±3.3 %	24.8 %
Spinel ($MgAl_2O_4$)	27.5±2.3 %	27.5±2.3 %	35.3 %
Major Fe phase	44.7± 3.5% (Fe)	44.7± 3.5% (FeO)	28.8 % (Fe_2O_3)
Minor reduced phases	5.7 % (FeS, Ni, Cu)	2.2 % (FeS)	2.9 % (FeS)
Minor oxides	2.9±0.3 % (CaO, Cr_2O_3, MnO)	6.4±0.6 % (CaO, Cr_2O_3, MnO, NiO, CuO)	8.2 % (CaO, Cr_2O_3, MnO, NiO, CuO)

References and Notes

1. P. C. Frisch, J. D. Slavin, Interstellar dust close to the Sun. *Earth Planets Space* **65**, 175–182 (2013). doi:10.5047/eps.2012.05.001

2. H. Kimura, I. Mann, E. K. Jessberger, Composition, structure, and size distribution of dust in the local interstellar cloud. *Astrophys. J.* **583**, 314–321 (2003). doi:10.1086/345102

3. B. T. Draine, Interstellar dust grains. *Annu. Rev. Astron. Astrophys.* **41**, 241–289 (2003). doi:10.1146/annurev.astro.41.011802.094840

4. M. Landgraf, W. J. Baggaley, E. Grun, H. Kruger, G. Linkert, Aspects of the mass distribution of interstellar dust grains in the solar system from in situ measurements. *J. Geophys. Res. Space Phys.* **105**, 10343–10352 (2000). doi:10.1029/1999JA900359

5. E. Grün, H. A. Zook, M. Baguhl, A. Balogh, S. J. Bame, H. Fechtig, R. Forsyth, M. S. Manner, M. Horanyi, J. Kissel, B.-A. Lindblad, D. Linkert, G. Linkert, I. Mann, J. A. M. McDonnell, G. E. Morfill, J. L. Phillips, C. Polanskey, G. Schwehm, N. Siddique, P. Staubach, J. Svestka, A. Taylor, Discovery of Jovian Dust Streams and Interstellar Grains by the Ulysses Spacecraft. *Nature* **362**, 428–430 (1993). doi:10.1038/362428a0

6. H. Krüger, V. Dikarev, B. Anweiler, S. F. Dermott, A. L. Graps, E. Grün, B. A. Gustafson, D. P. Hamilton, M. S. Hanner, M. Horányi, J. Kissel, D. Linkert, G. Linkert, I. Mann, J. A. M. McDonnell, G. E. Morfill, C. Polanskey, G. Schwehm, R. Srama, Three years of Ulysses dust data: 2005 to 2007. *Planet. Space Sci.* **58**, 951–964 (2010). doi:10.1016/j.pss.2009.11.002

7. All particle sizes heareafter are given in diameter, rather than radius.

8. D. Brownlee, P. Tsou, J. Aléon, C. M. Alexander, T. Araki, S. Bajt, G. A. Baratta, R. Bastien, P. Bland, P. Bleuet, J. Borg, J. P. Bradley, A. Brearley, F. Brenker, S. Brennan, J. C. Bridges, N. D. Browning, J. R. Brucato, E. Bullock, M. J. Burchell, H. Busemann, A. Butterworth, M. Chaussidon, A. Cheuvront, M. Chi, M. J. Cintala, B. C. Clark, S. J. Clemett, G. Cody, L. Colangeli, G. Cooper, P. Cordier, C. Daghlian, Z. Dai, L. D'Hendecourt, Z. Djouadi, G. Dominguez, T. Duxbury, J. P. Dworkin, D. S. Ebel, T. E. Economou, S. Fakra, S. A. Fairey, S. Fallon, G. Ferrini, T. Ferroir, H. Fleckenstein, C. Floss, G. Flynn, I. A. Franchi, M. Fries, Z. Gainsforth, J. P. Gallien, M. Genge, M. K. Gilles, P. Gillet, J. Gilmour, D. P. Glavin, M. Gounelle, M. M. Grady, G. A. Graham, P. G. Grant, S. F. Green, F. Grossemy, L. Grossman, J. N. Grossman, Y. Guan, K. Hagiya, R. Harvey, P. Heck, G. F. Herzog, P. Hoppe, F. Hörz, J. Huth, I. D. Hutcheon, K. Ignatyev, H. Ishii, M. Ito, D. Jacob, C. Jacobsen, S. Jacobsen, S. Jones, D. Joswiak, A. Jurewicz, A. T. Kearsley, L. P. Keller, H. Khodja, A. L. Kilcoyne, J. Kissel, A. Krot, F. Langenhorst, A. Lanzirotti, L. Le, L. A. Leshin, J. Leitner, L. Lemelle, H. Leroux, M. C. Liu, K. Luening, I. Lyon, G. Macpherson, M. A. Marcus, K. Marhas, B. Marty, G. Matrajt, K. McKeegan, A. Meibom, V. Mennella, K. Messenger, S. Messenger, T. Mikouchi, S. Mostefaoui, T. Nakamura, T. Nakano, M. Newville, L. R. Nittler, I. Ohnishi, K. Ohsumi, K. Okudaira, D. A. Papanastassiou, R. Palma, M. E. Palumbo, R. O. Pepin, D. Perkins, M. Perronnet, P. Pianetta, W. Rao, F. J. Rietmeijer, F. Robert, D. Rost, A. Rotundi, R. Ryan, S. A. Sandford, C. S. Schwandt, T. H. See, D. Schlutter, J. Sheffield-Parker, A. Simionovici, S. Simon, I. Sitnitsky, C. J. Snead, M. K. Spencer, F. J. Stadermann, A. Steele, T. Stephan, R. Stroud, J. Susini, S. R. Sutton, Y. Suzuki, M.

Taheri, S. Taylor, N. Teslich, K. Tomeoka, N. Tomioka, A. Toppani, J. M. Trigo-Rodríguez, D. Troadec, A. Tsuchiyama, A. J. Tuzzolino, T. Tyliszczak, K. Uesugi, M. Velbel, J. Vellenga, E. Vicenzi, L. Vincze, J. Warren, I. Weber, M. Weisberg, A. J. Westphal, S. Wirick, D. Wooden, B. Wopenka, P. Wozniakiewicz, I. Wright, H. Yabuta, H. Yano, E. D. Young, R. N. Zare, T. Zega, K. Ziegler, L. Zimmerman, E. Zinner, M. Zolensky, Comet 81P/Wild 2 under a microscope. *Science* **314**, 1711–1716 (2006). Medline doi:10.1126/science.1135840

9. A. J. Westphal *et al*., Stardust Interstellar Preliminary Examination I: Identification of tracks in aerogel. *Meteorit. Planet. Sci.* 10.1111/maps.12168 (2014).

10. D. R. Frank *et al*., Stardust Interstellar Preliminary Examination II: Curating the interstellar dust collector, picokeystones, and sources of impact tracks. *Meteorit. Planet. Sci.* 10.1111/maps.12147 (2014).

11. H. A. Bechtel *et al*., Stardust Interstellar Preliminary Examination III: Infrared spectroscopic analysis of interstellar dust candidates. *Meteorit. Planet. Sci.* 10.1111/maps.12125 (2014).

12. A. L. Butterworth *et al*., Stardust Interstellar Preliminary Examination IV: Scanning Transmission X-ray Microscopy analyses of impact features in the Stardust Interstellar Dust Collector. *Meteorit. Planet. Sci.* 10.1111/maps.12220 (2014).

13. F. E. Brenker *et al*., Stardust Interstellar Preliminary Examination V: XRF analyses of interstellar dust candidates at ESRF ID13. *Meteorit. Planet. Sci.* 10.1111/maps.12206 (2014).

14. A. S. Simionovici *et al*., Stardust Interstellar Preliminary Examination VI: Quantitative elemental analysis by synchrotron X-ray fluorescence nanoimaging of eight impact features in aerogel. *Meteorit. Planet. Sci.* 10.1111/maps.12208 (2014).

15. G. J. Flynn *et al*., Stardust Interstellar Preliminary Examination VII: Synchrotron X-ray fluorescence analysis of six stardust interstellar candidates measured with the advanced photon source 2-ID-D microprobe. *Meteorit. Planet. Sci.* 10.1111/maps.12144 (2014).

16. Z. Gainsforth *et al*., Stardust Interstellar Preliminary Examination VIII: Identification of crystalline material in two interstellar candidates. *Meteorit. Planet. Sci.* 10.1111/maps.12148 (2014).

17. F. Postberg *et al*., Stardust Interstellar Preliminary Examination IX: High-speed interstellar dust analog capture in Stardust flight-spare aerogel. *Meteorit. Planet. Sci.* 10.1111/maps.12173 (2014).

18. V. J. Sterken *et al*., Stardust Interstellar Preliminary Examination X: Impact speeds and directions of interstellar grains on the Stardust dust collector. *Meteorit. Planet. Sci.* 10.1111/maps.12219 (2014).

19. R. M. Stroud *et al*., Stardust Interstellar Preliminary Examination XI: Identification and elemental analysis of impact craters on Al foils from the Stardust Interstellar Dust Collector. *Meteorit. Planet. Sci.* 10.1111/maps.12136 (2014).

20. A. J. Westphal *et al*., Final reports of the Stardust Interstellar Preliminary Examination. *Meteorit. Planet. Sci.* 10.1111/maps.12221 (2014).

21. Supplementary details are available on *Science* Online.

22. R. Lallement, J. L. Bertaux, On the decades-long stability of the interstellar wind through the solar system. *Astron. Astrophys.* **565**, A41 (2014). doi:10.1051/0004-6361/201323216

23. M. C. Price, A. T. Kearsley, M. J. Burchell, F. Hörz, J. Borg, J. C. Bridges, M. J. Cole, C. Floss, G. Graham, S. F. Green, P. Hoppe, H. Leroux, K. K. Marhas, N. Park, R. Stroud, F. J. Stadermann, N. Telisch, P. J. Wozniakiewicz, Comet 81P/Wild 2: The size distribution of finer (sub-10 μm) dust collected by the Stardust spacecraft. *Meteorit. Planet. Sci.* **45**, 1409–1428 (2010). doi:10.1111/j.1945-5100.2010.01104.x

24. M. C. Price, A. T. Kearsley, M. J. Burchell, L. E. Howard, J. K. Hillier, N. A. Starkey, P. J. Wozniakiewicz, M. J. Cole, Stardust interstellar dust calibration: Hydrocode modeling of impacts on Al-1100 foil at velocities up to 300 km s^{-1} and validation with experimental data. *Meteorit. Planet. Sci.* **47**, 684–695 (2012). doi:10.1111/j.1945-5100.2011.01300.x

25. A. T. Kearsley, J. Borg, G. A. Graham, M. J. Burchell, M. J. Cole, H. Leroux, J. C. Bridges, F. Hörz, P. J. Wozniakiewicz, P. A. Bland, J. P. Bradley, Z. R. Dai, N. Teslich, T. See, P. Hoppe, P. R. Heck, J. Huth, F. J. Stadermann, C. Floss, K. Marhas, T. Stephan, J. Leitner, Dust from comet Wild 2: Interpreting particle size, shape, structure, and composition from impact features on the Stardust aluminum foils. *Meteorit. Planet. Sci.* **43**, 41–73 (2008). doi:10.1111/j.1945-5100.2008.tb00609.x

26. A. J. Westphal, C. Snead, A. Butterworth, G. A. Graham, J. P. Bradley, S. Bajt, P. G. Grant, G. Bench, S. Brennan, P. Pianetta, Aerogel keystones: Extraction of complete hypervelocity impact events from aerogel collectors. *Meteorit. Planet. Sci.* **39**, 1375–1386 (2004). doi:10.1111/j.1945-5100.2004.tb00952.x

27. P. Tsou, D. E. Brownlee, S. A. Sandford, F. Horz, M. E. Zolensky, Wild 2 and interstellar sample collection and Earth return. *J. Geophys. Res. Planets* **108**, 8113 (2003). doi:10.1029/2003JE002109

28. S. A. Sandford, S. Bajt, S. J. Clemett, G. D. Cody, G. Cooper, B. T. Degregorio, V. De VERA, J. P. Dworkin, J. E. Elsila, G. J. Flynn, D. P. Glavin, A. Lanzirotti, T. Limero, M. P. Martin, C. J. Snead, M. K. Spencer, T. Stephan, A. Westphal, S. Wirick, R. N. Zare, M. E. Zolensky, Assessment and control of organic and other contaminants associated with the Stardust sample return from comet 81P/Wild 2. *Meteorit. Planet. Sci.* **45**, 406–433 (2010). doi:10.1111/j.1945-5100.2010.01031.x

29. J. P. Bradley, Chemically anomalous, preaccretionally irradiated grains in interplanetary dust from comets. *Science* **265**, 925–929 (1994). Medline doi:10.1126/science.265.5174.925

30. L. P. Keller, S. Messenger, On the origins of GEMS grains. *Geochim. Cosmochim. Acta* **75**, 5336–5365 (2011). doi:10.1016/j.gca.2011.06.040

31. P. C. Frisch, M. Bzowski, G. Livadiotis, D. J. McComas, E. Moebius, H. R. Mueller, W. R. Pryor, N. A. Schwadron, J. M. Sokół, J. V. Vallerga, J. M. Ajello, Decades-long changes of the interstellar wind through our solar system. *Science* **341**, 1080–1082 (2013). Medline doi:10.1126/science.1239925

32. V. Dikarev, E. Grün, M. Landgraf, W. J. Baggaley, D. P. Galligan, in *Proceedings of the Meteoroids 2001 Conference,* B. Warmbein, Ed. (2001), vol. 495, pp. 609–615.

33. M. Landgraf, M. Müller, E. Grün, Prediction of the in-situ dust measurements of the Stardust mission to comet 81P/Wild 2. *Planet. Space Sci.* **47**, 1029–1050 (1999). doi:10.1016/S0032-0633(99)00031-8

34. M. J. Burchell, M. J. Cole, M. C. Price, A. T. Kearsley, Experimental investigation of impacts by solar cell secondary ejecta on silica aerogel and aluminum foil: Implications for the Stardust Interstellar Dust Collector. *Meteorit. Planet. Sci.* **47**, 671–683 (2012). doi:10.1111/j.1945-5100.2011.01294.x

35. N. Gehrels, Confidence limits for small number events in astrophysical data. *Astrophys. J.* **303**, 336–346 (1986). doi:10.1086/164079

36. H. Krüger, E. Grün, Interstellar dust inside and outside the heliosphere. *Space Sci. Rev.* **143**, 347–356 (2009). doi:10.1007/s11214-008-9431-3

37. M. Min, J. W. Hovenier, L. B. F. M. Waters, A. de Koter, The infrared emission spectra of compositionally inhomogeneous aggregates composed of irregularly shaped constituents. *Astron. Astrophys.* **489**, 135–141 (2008). doi:10.1051/0004-6361:200809534

38. E. B. Jenkins, A unified representation of gas-phase element depletions in the interstellar medium. *Astrophys. J.* **700**, 1299–1348 (2009). doi:10.1088/0004-637X/700/2/1299

39. F. Kemper, W. J. Vriend, A. G. G. M. Tielens, The absence of crystalline silicates in the diffuse interstellar medium. *Astrophys. J.* **609**, 826–837 (2004). doi:10.1086/421339

40. F. Kemper, W. J. Vriend, A. Tielens, Errata: The absence of crystalline silicates in the diffuse interstellar medium (**609**, p. 826, 2004). *Astrophys. J.* **633**, 534–534 (2005). doi:10.1086/447764

41. A. P. Jones, J. A. Nuth III, Dust destruction in the ISM: A re-evaluation of dust lifetimes. *Astron. Astrophys.* **530**, A44 (2011). doi:10.1051/0004-6361/201014440

42. F. J. Molster, L. Waters, The mineralogy of interstellar and circumstellar dust. *Astromineralogy* **609**, 121–170 (2003). doi:10.1007/3-540-45840-9_3

43. S. Messenger, L. P. Keller, D. S. Lauretta, Supernova olivine from cometary dust. *Science* **309**, 737–741 (2005). Medline doi:10.1126/science.1109602

44. C. Vollmer, P. Hoppe, F. E. Brenker, C. Holzapfel, Stellar $MgSiO_3$ perovskite: A shock-transformed stardust silicate found in a meteorite. *Astrophys. J.* **666**, L49–L52 (2007). doi:10.1086/521623

45. B. T. Draine, Perspectives on interstellar dust inside and outside of the heliosphere. *Space Sci. Rev.* **143**, 333–345 (2009). doi:10.1007/s11214-008-9411-7

46. D. Nesvorny, P. Jenniskens, H. F. Levison, W. F. Bottke, D. Vokrouhlicky, M. Gounelle, Cometary origin of the Zodiacal cloud and carbonaceous micrometeorites. Implications for hot debris disks. *Astrophys. J.* **713**, 816–836 (2010). doi:10.1088/0004-637X/713/2/816

47. D. Nesvorny, D. Vokrouhlicky, W. F. Bottke, M. Sykes, Physical properties of asteroid dust bands and their sources. *Icarus* **181**, 107–144 (2006). doi:10.1016/j.icarus.2005.10.022

48. D. Jewitt, H. Weaver, J. Agarwal, M. Mutchler, M. Drahus, A recent disruption of the main-belt asteroid P/2010 A2. *Nature* **467**, 817–819 (2010). Medline doi:10.1038/nature09456

49. H. H. Hsieh, D. Jewitt, P. Lacerda, S. C. Lowry, C. Snodgrass, The return of activity in main-belt comet 133P/Elst-Pizarro. *Mon. Not. R. Astron. Soc.* **403**, 363–377 (2010). doi:10.1111/j.1365-2966.2009.16120.x

50. B. J. Gladman, D. R. Davis, C. Neese, R. Jedicke, G. Williams, J. J. Kavelaars, J.-M. Petit, H. Scholl, M. Holman, B. Warrington, G. Esquerdo, P. Tricarico, Sub-Kilometer Asteroid Diameter Survey (SKADS) V1.0. EAR-A-I0655-5-SKADS-V1.0. NASA Planetary Data System (2010).

51. E. Grün, H. A. Zook, H. Fechtig, R. H. Giese, Collisional balance of the meteoritic complex. *Icarus* **62**, 244–272 (1985). doi:10.1016/0019-1035(85)90121-6

52. R. L. Smith, K. M. Pontoppidan, E. D. Young, M. R. Morris, E. F. van Dishoeck, High-precision (CO)-O-17, (CO)-O-18, and (CO)-O-16 measurements in young stellar objects: Analogues for CO self-shielding in the early solar system. *Astrophys. J.* **701**, 163–175 (2009). doi:10.1088/0004-637X/701/1/163

53. E. D. Young, M. Gounelle, R. L. Smith, M. R. Morris, K. M. Pontoppidan, Astronomical oxygen isotopic evidence for supernova enrichment of the solar system birth environment by propagating star formation. *Astrophys. J.* **729**, 43 (2011). doi:10.1088/0004-637X/729/1/43

54. L. R. Nittler, E. Gaidos, Galactic chemical evolution and the oxygen isotopic composition of the solar system. *Meteorit. Planet. Sci.* **47**, 2031–2048 (2012). doi:10.1111/j.1945-5100.2012.01410.x

55. J. G. A. Wouterloot, C. Henkel, J. Brand, G. R. Davis, Galactic interstellar $^{18}O/^{17}O$ ratios - a radial gradient? *Astron. Astrophys.* **487**, 237–246 (2008). doi:10.1051/0004-6361:20078156

56. A. A. Penzias, The isotopic abundances of inter-stellar oxygen. *Astrophys. J.* **249**, 518–523 (1981). doi:10.1086/159311